Research Square

Preprints are preliminary reports that have not undergone peer review.
They should not be considered conclusive, used to inform clinical practice,
or referenced by the media as validated information.

Graviton Modes on the Kuhn Lattice: Euclidean Continuation and Lorentzian Propagation

Philip Beltracchi

pbeltracchi@recognitionphysics.org

Recognition Physics Research Institute https://orcid.org/0000-0002-4226-7796

Jonathan Washburn

Recognition Physics Research Institute https://orcid.org/0009-0001-8868-7497

Research Article

Keywords: Regge calculus, Quantum gravity, Graviton dispersion, Graviton Cherenkov 15 radiation

Posted Date: November 24th, 2026

DOI: https://doi.org/10.21203/rs.3.rs-11826151/v1

License: This work is licensed under a Creative Commons Attribution 4.0 International License.
Read Full License

Additional Declarations: The authors declare no competing interests.

Graviton Modes on the Kuhn Lattice: Euclidean Continuation and Lorentzian Propagation

Jonathan Washburn[1] and Philip Beltracchi[1*]

[1] Recognition Physics Institute, Austin, 80138, TX, USA.

*Corresponding author(s). E-mail(s): pbeltracchi@recognitionphysics.org;
Contributing authors: jon@recognitionphysics.org;

The linearized Regge action on the four-dimensional Kuhn lattice has a graviton branch on the zero set of the nearest-neighbor scalar Laplacian. We give the exact mode count at complex momentum, a geometric reason for the inert hypercube-diagonal strain, and the directional dispersion. With time along a coordinate axis, continuation of one momentum component gives two polarizations of phase speed $1-(1+\sum_j n_j^4)\mathrm{k}^2a^2/24+O(\mathrm{k}^4a^4)$ relative to the infrared speed, where n is the spatial direction. Their phase and group speeds remain below that speed throughout the spatial Brillouin zone, and both carry the scalar lattice Laplacian as their exact symbol at every momentum. Of the four edge-direction classes used as time, only axis time is real and subluminal in every spatial direction. Conversely, the same triangulation on a flat Lorentzian background $g_L = I_4 - J_4$ gives a different law. Along the paired spatial ray the cross and plus branches have phase speeds $1+5K^2/24+o(K^2)$ and $1-59K^2/24+o(K^2)$, with K the spatial wave number in lattice units; the Euclidean continuation has no such splitting. Two harmonic scalar sources fail independent null-space conditions of the Euclidean edge equations. For the axis-time continuation, conventional ultrarelativistic fermions and minimal gravitational coupling imply the conservative cosmic-ray bound $a < 1.42\times10^{-31}$ m. That bound is not transferred to the Lorentzian branches.

1 Introduction

Does a graviton dispersion law obtained by continuing a Euclidean lattice describe the waves of a Lorentzian lattice with the same connectivity? The distinction matters whenever a lattice correction is compared with an observed speed or used in a radiation bound. The Fourier symbol depends on the background edge geometry as well as

on the triangulation. We compute both constructions in a case where they can be compared exactly, and find different polarization behavior.

Regge calculus describes gravity through a piecewise flat simplicial geometry: edge intervals determine triangle areas and the deficit angles around them. In four dimensions the Euclidean action is $\sum_h A_h \delta_h$, corresponding to $\frac{1}{2}\int R\sqrt{g}\,\mathrm{d}^4x$ under suitable controlled refinement [1]. It is used in numerical relativity [2] and provides geometric ingredients for approaches including causal dynamical triangulations [3] and spin foams [4]. Fixed-lattice models also motivate searches for directional propagation effects [5, 6].

In this paper, we use the Kuhn triangulation of $\mathbb{Z}^4$: each unit hypercube is cut into the 24 simplices indexed by the orderings of the four coordinate directions [7, 8]. Every vertex carries 15 edge classes: 4 axes, 6 face diagonals, 4 body diagonals and 1 hypercube diagonal. Expanding the nearly flat Regge action to second order with respect to squared edge lengths, we define its Fourier transform $\mathsf{M}(k)$, which is a 15×15 matrix-valued trigonometric polynomial. The propagating waves are the k at which $\mathsf{M}(k)$ acquires null vectors beyond the ones forced by symmetry.

The weak-field limit of Regge calculus has been studied since the 1980s: Roček and Williams on this lattice [9, 10], Williams on Lorentzian lattice geometry [11], Feinberg, Friedberg, Lee and Ren near the continuum limit [5]; the reviews of Williams and Tuckey [12], Loll [13] and Hamber [14] survey the field.

The calculation has three connected parts: the exact Euclidean mode count, its comparison with a direct Lorentzian calculation, and the conditions needed to couple a source. The main results are as follows.

1. **A fifth zero mode, explained.** Besides the four translation (gauge) zero modes, $\mathsf{M}(k)$ annihilates the hypercube-diagonal strain at every k. Roček and Williams saw this mode in their fluctuation matrix [10]. We explain the geometric reason: every triangle of the Kuhn triangulation is right-angled, the hypercube diagonal is always the hypotenuse, and the area of a right triangle is stationary in its hypotenuse (Theorem 3.1).
2. **An isotropic quadratic sector.** After the four non-metric strain directions are eliminated, the quadratic part of the symbol on the ten metric perturbations is the linearized Einstein operator: eigenvalue $-\frac{1}{4}|k|^2$ on a five-dimensional Euclidean transverse-traceless subspace, 0 on four gauge directions, $+\frac{1}{2}|k|^2$ on the transverse trace, for every direction of k (Theorem 3.4).
3. **An exact branch.** The transverse-traceless (TT) branch is $\mathcal{L}(k) = \sum_{\mu=1}^{4} 4\sin^2(k_\mu/2) = 0$, the nearest-neighbor Laplacian, to all orders in lattice momentum within the quadratic action, for both polarizations, and no other wave vector carries a propagating mode (Theorem 4.2). The proof uses the finite-difference factorization of the lattice weak-field action by Roček and Williams [9, 10], which holds here as an exact identity of rational functions in the edge variables at every complex momentum; root finding directly in the edge variables reproduces its roots to 10^{-40} as an independent check.
4. **A direction-dependent, subluminal cone.** We define a Wick-rotated propagation vector with time T along one of the edge classes and $\hat{n} \perp T$ the

propagation direction. The phase velocity is $1 - \kappa(\hat{n})\mathrm{k}^2 a^2$ with $\kappa = (1 + A)/24$, $A = \sum_j n_j^4 \in [1/3, 1]$. Among the edge-direction classes for time, we find the coordinate axis directions give a real branch below the infrared speed in every spatial direction while the other three classes admit a speed above that limit or a complex frequency (Theorems 5.1, 5.4). With axis time the two polarizations carry the scalar symbol $\mathcal{L}(k)$ exactly, so this frequency is the decay rate of their Euclidean-time correlations (Proposition 5.2 and the following paragraph).

5. **A direct Lorentzian comparison.** On $g_L = I_4 - J_4$, with unit time along the hypercube diagonal, an exact calculation on the paired spatial ray gives a cross branch with coefficient $5/24$ and a plus branch with coefficient $-59/24$ in $v = 1 + cK^2 + o(K^2)$ (Section 6). The Euclidean continuation remains polarization-degenerate, including along the corresponding diagonal time direction.
6. **Two source-compatibility obstructions.** A scalar action on the same Euclidean edge geometry has harmonic fields whose edge sources fail the null-space conditions of the gravitational Hessian. One obstruction uses the inert diagonal; the other survives its removal and uses a vertex-displacement mode (Section 7).
7. **A conditional bound on the spacing.** The gravitational refractive index is $n_g = 1 + (1 + A)\mathrm{k}^2 a^2/24 + O(\mathrm{k}^4 a^4)$. If the emitting matter has conventional dispersion and minimal gravitational coupling, the cosmic-ray analysis of Kostelecký and Tasson [15] gives $a < 1.42 \times 10^{-31}$ m (Section 8).

The finite-difference factorization and its scalar Laplacian factor are explicit in the work of Roček and Williams and its presentation by Hamber [9, 10, 14]. The additions here are the geometric explanation of the inert mode, the complete complex rank argument, exact continuation and speed formulas, and their comparison with a directly assembled Lorentzian operator. The scalar examples identify a separate consistency condition that a vacuum dispersion calculation cannot supply. The cosmic-ray bound is an application under specified matter assumptions; it is not a consequence of the graviton characteristic set alone.

Sections 2–4 develop the Euclidean Hessian and count its modes. Section 5 studies its time continuations. Section 6 constructs the direct Lorentzian comparison, and Section 7 develops the source-compatibility conditions. Sections 8 and 9 give the conditional phenomenology and a candidate spacing. The appendices specify the Lorentzian matrices and the Euclidean computational material. Table 1 records the notation used in the Euclidean calculation.

2 The lattice and the linearized action

2.1 The Kuhn triangulation

Take the vertices $\mathbb{Z}^4$. For each permutation π of $\{1, 2, 3, 4\}$ and each $x \in \mathbb{Z}^4$ the simplex $\sigma_{x,\pi}$ has vertices $v_0 = x$, $v_j = v_{j-1} + e_{\pi(j)}$, $j = 1, \ldots, 4$: a path along the edges of the unit hypercube at x visiting one axis at a time. The 24 simplices at a given x tile the hypercube, and the tiling is a triangulation of $\mathbb{R}^4$ [7, 8]. The edge from v_i to v_j $(i < j)$ is the vector $D = e_{\pi(i+1)} + \cdots + e_{\pi(j)}$, a 0–1 vector with $j - i$ ones. Every nonzero $D \in \{0, 1\}^4$ occurs, so there are 15 edge classes per vertex, with squared lengths

Term	Meaning in this paper
Kuhn triangulation	The cut of each unit hypercube of $\mathbb{Z}^4$ into 24 simplices, one per ordering of the four axes.
Edge class D	A nonzero vector $D \in \{0,1\}^4$; the edge from x to $x + D$; squared length $\lvert D\rvert^2 \in \{1,2,3,4\}$.
Hinge	A triangle; the deficit angle lives on hinges in four dimensions.
Symbol $\mathsf{M}(k)$	The Fourier transform of the Hessian of the Regge action at flat space; a 15×15 matrix of trigonometric polynomials, real symmetric for real momentum.
Metric strains	The 10-dimensional image of a symmetric 4×4 tensor h under $h \mapsto (D^{\mathsf{T}} h D)_D$; its coordinate vector is $x = \mathrm{vec}_F\, h$.
Reduced symbol $\mathsf{E}(k)$	The quadratic form of $\mathsf{M}(k)$ restricted to metric strains after the 4 non-metric strain directions are eliminated at their stationary point (a Schur complement); a 10×10 matrix acting on $x = \mathrm{vec}_F\, h$.
Gauge modes	Strains produced by moving vertices; exact null vectors of $\mathsf{M}(k)$ for every k.
TT branch	The nonzero complex momenta where the interacting edge symbol has two null modes modulo gauge; these approach continuum TT tensors in the infrared.
$\mathcal{L}(k)$	$\sum_{\mu=1}^{4} 4\sin^2(k_\mu/2)$, the symbol of the nearest-neighbor Laplacian.
$A(\hat{n})$	$\sum_{j=1}^{3} n_j^4$ for a unit spatial direction; 1 on an axis, 1/2 on a face diagonal, 1/3 on a body diagonal, mean 3/5.
$s^{(6)}$	The dimension-six graviton coefficients of the Standard-Model Extension; $s^{(6)}_{jm}$ their spherical components.
k, k, K	$\mathbb{C}^4$ Bloch wave vector, modulus of the 3D spatial wavenumber in the complexified Euclidean case, modulus of the spatial wavenumber in the Lorentzian case.

Table 1 Terms used throughout. Lattice units $a = 1$ are used in Sections 2–5; a is restored in Section 8.

$|D|^2 = 1, 2, 3, 4$ for 4 axis, 6 face diagonal, 4 body diagonal, and 1 hypercube diagonal classes respectively (Figure 1). There are 50 triangle classes per vertex (ordered pairs of disjoint nonempty 0–1 vectors: $3^4 - 2 \cdot 2^4 + 1$), and 60 tetrahedra.

Lemma 2.1 (right triangles)**.** *Every triangle of the Kuhn triangulation has edge vectors $D^\mu_{(1)}$, $D^\mu_{(2)}$, $D^\mu_{(1)} + D^\mu_{(2)}$ with $D^\mu_{(1)}, D^\mu_{(2)} \in \{0,1\}^4$ of disjoint support. It is right-angled at the vertex between $D^\mu_{(1)}$ and $D^\mu_{(2)}$, with area $\frac{1}{2}|D_{(1)}||D_{(2)}|$. The hypercube diagonal $(1,1,1,1)$ occurs only as a hypotenuse.*

Proof The edges $D^\mu_{(1)}$ and $D^\mu_{(2)}$ must have disjoint support because otherwise $D^\mu_{(1)} + D^\mu_{(2)}$ would leave the hypercube. Because $D^\mu_{(1)}$ and $D^\mu_{(2)}$ are sums of disjoint sets of axis vectors, $D^\mu_{(1)} D_{(2)\mu} = 0$. The area of a right triangle is half the area of the corresponding rectangle, that is $1/2|D_{(1)}||D_{(2)}|$. The diagonal $(1,1,1,1)$ has full support and cannot be a leg, since a leg must leave room for a disjoint nonempty $D^\mu_{(2)}$. □

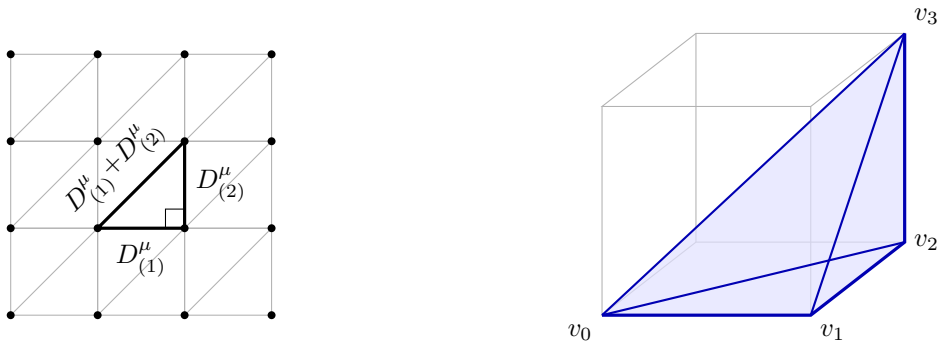

(a) $d = 2$ (b) $d = 3$

Fig. 1 The Kuhn triangulation. (a) In two dimensions: three edge classes per vertex and one right triangle per half square; the triangle $D^\mu_{(1)}, D^\mu_{(2)}, D^\mu_{(1)}+D^\mu_{(2)}$ has its right angle between the two legs. (b) In three dimensions: the tetrahedron $v_0v_1v_2v_3$ for the ordering $(1, 2, 3)$, one of the six that tile the cube. In d dimensions each unit cube is cut into $d!$ simplices, one for each order in which the axes are traversed; every triangle has edge vectors $D^\mu_{(1)}$, $D^\mu_{(2)}$, $D^\mu_{(1)} + D^\mu_{(2)}$ with $D^\mu_{(1)}D_{(2)\mu} = 0$ and is right-angled, and in four dimensions the hypercube diagonal is a hypotenuse in every triangle that contains it.

2.2 The Regge action and its Hessian at flat space

Let $a_e = \ell_e^2$ be the squared length of edge e. The Regge action is

$$S[a] = \kappa \sum_h A_h(a)\, \delta_h(a), \qquad \delta_h = 2\pi - \sum_{\sigma \ni h} \theta_{h,\sigma}(a), \tag{1}$$

the sum over hinges (triangles) of area times deficit angle, the deficit being 2π minus the sum of the dihedral angles at h in the simplices containing it. At the flat configuration $a_e = |D_e|^2$ every deficit vanishes. While Regge arrived at this action through other arguments, it is noteworthy that the only continuous setup $S = \sum_h f(A_h, \delta_h)$ obeying additivity in area[1] $f(A_1+A_2, \delta) = f(A_1, \delta)+f(A_2, \delta)$ and in the deficit, $f(A, \delta_1+\delta_2) = f(A, \delta_1)+f(A, \delta_2)$, is $f = \kappa A\delta$. The constant κ is important for coupled systems, but in this work we are looking at vacuum gravitational waves so it is set to 1 for convenience.

The first variation of the Regge action is thus $\mathrm{d}S = \sum_h A_h \mathrm{d}\delta_h + \sum_h \mathrm{d}A_h\delta_h$. The Schläfli identity $\sum_h A_h\, \mathrm{d}\delta_h = 0$ holds at every configuration [1, 14]. Further, $\sum_h \delta_h\, \mathrm{d}A_h$ vanishes at flat space because the deficit angles are zero, so the first order variation vanishes.

The second variation is

$$\mathrm{d}_e\mathrm{d}_{e'}S = \sum_h \delta_h \mathrm{d}_e\mathrm{d}_{e'}A_h + \sum_h \mathrm{d}_e\delta_h\mathrm{d}_{e'}A_h + \sum_h \mathrm{d}_{e'}\delta_h\mathrm{d}_eA_h + \sum_h A_h\mathrm{d}_e\mathrm{d}_{e'}\delta_h, \tag{2}$$

[1] Additivity in area could, for a general triangulation, be motivated by noticing that a triangular hinge can be freely divided into smaller triangles.

where e, e' label the (not necessarily distinct) edges being perturbed. The first term again cancels from the deficit angle, and varying the Schläfli identity gives

$$\sum_h \mathrm{d}_e A_h \mathrm{d}_{e'} \delta_h + \sum_h A_h \mathrm{d}_e \mathrm{d}_{e'} \delta_h = 0, \tag{3}$$

so only one term from the second variation survives. Writing this as a Hessian gives

$$\mathsf{H}_{ee'} = \mathsf{H}_{e'e} = \frac{\partial^2 S}{\partial a_e \, \partial a_{e'}}\Big|_{\text{flat}} = \sum_h \frac{\partial A_h}{\partial a_{e'}} \frac{\partial \delta_h}{\partial a_e}. \tag{4}$$

The Euclidean flat simplices have strictly positive Gram determinants and nondegenerate triangular faces. In a neighborhood of the flat space lengths, the areas, interior dihedral angles, and finite local action are smooth functions of the squared lengths, so mixed derivatives commute and H is symmetric. The area gradient follows from Heron's formula,

$$16A^2 = 2(a_1 a_2 + a_2 a_3 + a_3 a_1) - (a_1^2 + a_2^2 + a_3^2). \tag{5}$$

The deficit gradient is the sum of dihedral-angle gradients, computed from the Gram determinants of the simplices. Both are algebraic numbers at flat space and are evaluated exactly (Appendix B). Because $\mathsf{H}_{ee'}$ vanishes unless e and e' share a simplex, the Hessian is a translation-invariant finite-range operator on the 15 edge fields.

2.3 The symbol

Write the edge perturbation as a plane wave in the midpoint convention,

$$\mathrm{d}a_D(x) = c_D \, e^{\mathrm{i}k\cdot(x+x_0+D/2)} \tag{6}$$

for the edge of class D at vertex x and a possible global offset x_0. Treat edge e as coming off the origin, then the second variation perturbing two edges e, e' can be written

$$\frac{1}{2} \sum_h (\mathrm{d}(a_e(0)))^* \frac{\partial A_h}{\partial a_e} \frac{\partial \delta_h}{\partial a_{e'}} \mathrm{d}a_{e'}(x), \tag{7}$$

where we are summing over all hinges in the complex. Notice that the factor $(\mathrm{d}(a_e(0)))^* \mathrm{d}a_{e'}(x)$ simplifies to $c_D^* c_{D'} e^{\mathrm{i}k\cdot(x+(D'-D)/2)}$; any global offset cancels. We can then describe how the Hessian acts on the 15 amplitudes c_D by

$$\mathsf{M}(k)_{DD'} = \sum_{x\in\mathbb{Z}^4} \mathsf{H}_{(D,0),(D',x)} \, e^{\mathrm{i}k\cdot(x+(D'-D)/2)}. \tag{8}$$

Each entry is a finite sum of exponentials in k; there are 302 nonzero terms in all, and it can be analytically extended to complex k. The second-order action of a plane wave with amplitude vector c is $\frac{1}{2} c^\dagger \mathsf{M}(k) c$ per unit cell, so the equations of motion at wave

vector k read $\mathsf{M}(k)c = 0$, and the propagating modes are the k at which $\mathsf{M}(k)$ has null vectors beyond those forced by symmetry. Three properties are immediate.

Lemma 2.2. *(i)* $\mathsf{M}(k)$ *is real and symmetric for real* k *and even in* k*; (ii)* $\mathsf{M}(gk) = \Pi_g \mathsf{M}(k) \Pi_g^{\mathsf{T}}$ *for every* g *in the symmetry group of the Kuhn triangulation, which is the group of order* 48 *generated by the permutations of the four axes and the inversion* $x \mapsto -x$ *(a single coordinate reflection sends the edge* $(1,1,0,0)$ *to* $(-1,1,0,0)$*, which is not an edge, so the full hyperoctahedral group does not act),* Π_g *the induced permutation of edge classes; (iii) for every* $\xi \in \mathbb{C}^4$ *the gauge vector*

$$g_\xi(k)_D = 4\mathrm{i}\,(D \cdot \xi)\,\sin(k \cdot D/2) \tag{9}$$

satisfies $\mathsf{M}(k) g_\xi(k) = 0$.

Proof (i) The midpoint convention makes the coupling between $(D, 0)$ and (D', x) depend on $x + (D' - D)/2$, the vector between the two edge midpoints; the reflection $x \mapsto -x$ of the lattice maps the Kuhn triangulation to itself and sends this vector to its negative, so the coefficients of $e^{\mathrm{i}k\cdot v}$ and $e^{-\mathrm{i}k\cdot v}$ are equal and M is a sum of cosines.
(ii) is the covariance of the action under the lattice symmetries.
(iii) Move each vertex at x by $\xi\, e^{\mathrm{i}k\cdot x}$. Assign the length vector between perturbed vertex x and the next perturbed vertex along a direction D as the difference of the perturbed vertex coordinates $\ell_g = (x + D + \xi e^{\mathrm{i}k\cdot(x+D)}) - (x + \xi e^{\mathrm{i}k\cdot(x)}) = D + \xi(e^{\mathrm{i}k\cdot(x+D)} - e^{\mathrm{i}k\cdot(x)})$. Squaring this to get a squared length gives

$$a_g = D^2 + 2D \cdot \xi(e^{\mathrm{i}k\cdot(x+D)} - e^{\mathrm{i}k\cdot(x)}) + O(\xi^2). \tag{10}$$

Rearranging the lowest order perturbation to be in line with the midpoint convention gives

$$da_g = 2D \cdot \xi e^{\mathrm{i}k\cdot(x+D/2)}(e^{\mathrm{i}k\cdot D/2} - e^{-\mathrm{i}k\cdot D/2}). \tag{11}$$

Recalling the form of (6) and selecting the c_D components as components of $g_\xi(k)$ gives (9). The displaced vertices remain embedded in flat Euclidean space[2] for small real displacements. Their deficits and action gradient vanish, so differentiating that gradient gives $\mathsf{M} g_\xi = 0$. The identity extends to complex momenta by analyticity. □

At $k = 0$ there are more zero modes beyond the $g_\xi(k)$. A constant metric perturbation $g_{\mu\nu} = \delta_{\mu\nu} + h_{\mu\nu}$ leaves the lattice flat and changes the squared lengths by $\mathrm{d}a_D = D^{\mathsf{T}} h D$; the strain vectors $\mathrm{P}\,\mathrm{vec}_F\, h := (D^{\mathsf{T}} h D)_D$, h ranging over symmetric 4×4 matrices, are therefore null vectors of $\mathsf{M}(0)$. The map P is injective (already its restriction to the four axes and six face diagonals, $a_i = 1 + h_{ii}$, $a_{ij} = 2 + h_{ii} + h_{jj} + 2h_{ij}$, is invertible), so its image, the space of metric strains, is ten-dimensional, and the components of h are coordinates on it.

Remark 2.3. So far, we have the 4-dimensional physical space and its associated vectors and tensors. We also have the 15-component c_D and 15×15 matrix $\mathsf{M}(k)$. However, it will be convenient to consider additional structures, which we list in Table 2. The first

[2] It is noteworthy that the same sorts of gauge invariance notions do not work in Regge calculus on curved backgrounds [16].

is the 14-component subspace of the edge amplitudes ignoring the nondynamical hypercube diagonal. Another convenient structure is the listing of the 10 independent components of a symmetric 4×4 tensor m as a vector, we use two different ways to do this. The ordering/indexing convention is $(x_{1,1}, x_{2,2}, x_{3,3}, x_{4,4}, x_{1,2}, x_{1,3}, x_{1,4}, x_{2,3}, x_{2,4}, x_{3,4}) \to (v_1, v_2, v_3, v_4, v_5, v_6, v_7, v_8, v_9, v_{10})$ in both cases. However, in certain cases we use the Frobenius normalization $x_{\mu\mu} = m_{\mu\mu}$, $x_{\mu\nu} = \sqrt{2}\, m_{\mu\nu}$ for $\mu < \nu$, so that $|x|^2 = \sum_{\mu\nu} m_{\mu\nu}^2$ for real m. We write $x = \mathrm{vec}_F(m)$ in this case. Alternatively, there are other cases where it is more convenient to not scale by the square root; $y_{\mu\mu} = m_{\mu\mu}$, $y_{\mu\nu} = m_{\mu\nu}$ for $\mu < \nu$. These alternate cases will be labeled $y = \mathrm{vec}_P(m)$. For complex momenta the continued quadratic forms use the bilinear transpose, not complex conjugation ($u \cdot u = u^T u$ rather than $u^\dagger u$).

Space	Dim	Elements and coordinates
$\mathcal{A}$	15	All edge-class amplitudes $c_D = \mathrm{d}a_D$. Home of $\mathsf{M}(k)$.
$\mathcal{A}'$	14	$\mathcal{A}$ without the hypercube diagonal. Home of $\mathsf{M}'(k)$.
$\mathcal{A}_{\mathrm{af}}$	10	The four axis and six face classes. Home of $\mathsf{R}(k)$.
$\mathcal{A}_{\mathrm{bd}}$	4	The four body diagonals.
$\mathcal{M}$	10	Symmetric 4×4 tensors h. Coordinates $x = \mathrm{vec}_F\, h$ or $y = \mathrm{vec}_P\, h$. Home of $\mathsf{E}(k)$, V, $\mathsf{K}(k)$.
$\mathcal{G}$	4	Vertex displacements ξ; also the target of the constraint $\mathsf{C}(k)$.
$\mathcal{A}_\sigma$	10	The ten edges of one labeled pentachoron, ordered by vertex pairs $(01, 02, 03, 04, 12, 13, 14, 23, 24, 34)$. Home of the cell matrix Z. This is not $\mathcal{A}_{\mathrm{af}}$ and not $\mathcal{M}$: the list includes two body diagonals and the hypercube diagonal.

Table 2 The seven vector spaces. $P : \mathcal{M} \to \mathcal{A}'$ and $Q : \mathbb{C}^4 \to \mathcal{A}'$ are the hypercube restricted metric-strain map and its complement; $N : \mathcal{A}_{\mathrm{af}} \to \mathcal{A}'$ and $O : \mathcal{A}_{\mathrm{bd}} \to \mathcal{A}'$ are the two coordinate inclusions; $\mathsf{W} : \mathcal{M} \to \mathcal{A}_{\mathrm{af}}$ and $\mathsf{C} : \mathcal{M} \to \mathcal{G}$. The cell matrix Z acts on $\mathcal{A}_\sigma$, the edges of a single pentachoron.

3 Zero modes and the quadratic sector

3.1 The hypotenuse mode

Theorem 3.1 (hypotenuse zero mode)**.** *Let e_{1111} be the unit vector on the hypercube-diagonal edge class. Then $\mathsf{M}(k)e_{1111} = 0$ for every $k \in \mathbb{C}^4$. Equivalently, the row and column of the Hessian (4) belonging to any hypercube diagonal vanish identically.*

Proof By Lemma 2.1, in every triangle containing a hypercube diagonal, that edge is the hypotenuse: $a_3 = a_1 + a_2$. From Heron's formula, $\partial(16A^2)/\partial a_3 = 2(a_1 + a_2) - 2a_3$, which is zero on a right triangle. So $\partial A_h/\partial a_e = 0$ for every hinge h when e is a hypercube diagonal,

and the row $\mathsf{H}_{e\,\cdot}$ in (4) vanishes. The column vanishes by the symmetry of H. Summing the zero rows with phases gives $\mathsf{M}(k)e_{1111} = 0$. □

Note that the deficit gradient $\partial\delta_h/\partial a_{1111}$ does not vanish: it has 54 nonzero entries over the 50 hinge classes. The hypercube diagonal mode is killed by the area gradient and symmetry of H. The 15 edge fields thus split, at linear order about flat space, into 14 that interact and one that does not. The hypercube diagonal does matter in higher order considerations and the full nonlinear Regge action, and its vanishing at lowest order provides nontrivial constraints for coupled systems (see Section 7).

Proposition 3.2 (zero-momentum kernel)**.** $\dim\ker\mathsf{M}(0) = 11$*: ten metric strains and the hypotenuse mode.*

Proof In addition to the counting argument (10 strains + 1 hypotenuse), explicitly constructing $\mathsf{M}(0)$ gives a matrix with characteristic polynomial

$$C(\lambda) = \lambda^{11}(\lambda+2)^3(\lambda+8) \tag{12}$$

The ten metric strains and e_{1111} are independent: a metric strain vanishing on the axes and face diagonals has $h = 0$, so it cannot equal e_{1111}. They therefore span the kernel. □

The supplementary exact-arithmetic program evaluates this polynomial from the coupling table. The nonzero-momentum count is derived in Section 4.

The block joining body diagonals to body diagonals has a k-independent self-coupling and no mutual cross terms: of the 302 couplings, exactly four join two body diagonals, and those are the diagonal entries; the block is $-\frac{1}{2}I_4$ at every k. The corresponding constant block is $18\,I_4$ of Roček and Williams [9, 14] with the opposite overall action sign. Their variable is the fractional strain $\epsilon_D = \mathrm{d}\ell_D/\ell_D$, so

$$\epsilon_D = \frac{\mathrm{d}a_D}{2\ell_D^2} = \frac{\mathrm{d}a_D}{2|D|^2}, \qquad -18\,\epsilon_D^2 = -\frac{18}{(2\cdot 3)^2}\,\mathrm{d}a_D^2 = -\tfrac{1}{2}\,\mathrm{d}a_D^2 \quad (|D|^2 = 3). \tag{13}$$

Figure 2 shows the two facts of this subsection side by side: the area of a triangle with fixed legs is stationary in its hypotenuse, and the symbol has one inert row and one constant block.

3.2 The reduced symbol and its quadratic part

Delete the inert hypotenuse row and column of M, writing the resulting 14×14 symbol as M'. Define P as P restricted to these rows: it is the 14×10 strain map $h \mapsto (D^{\mathsf{T}}hD)_D$ in Frobenius coordinates. Let Q be a 14×4 orthonormal basis of the complement of its image. In the basis (P, Q) the quadratic form $\frac{1}{2}c^{\mathsf{T}}\mathsf{M}'c$ has blocks $P^{\mathsf{T}}\mathsf{M}'P$, $P^{\mathsf{T}}\mathsf{M}'Q$, $Q^{\mathsf{T}}\mathsf{M}'Q$; the last is a 4×4 block which has eigenvalues $-8, -2, -2, -2$ at $k = 0$ (the characteristic polynomial of $\mathsf{M}'(0)$ can be inferred from the characteristic polynomial of M (12), from which the nonzero eigenvalues follow) and is invertible in a neighborhood. Label as E the Schur complement of the 4×4 block $Q^{\mathsf{T}}\mathsf{M}'Q$, that is

$$\mathsf{E}(k) = P^{\mathsf{T}}\mathsf{M}'P - P^{\mathsf{T}}\mathsf{M}'Q\,(Q^{\mathsf{T}}\mathsf{M}'Q)^{-1}Q^{\mathsf{T}}\mathsf{M}'P, \tag{14}$$

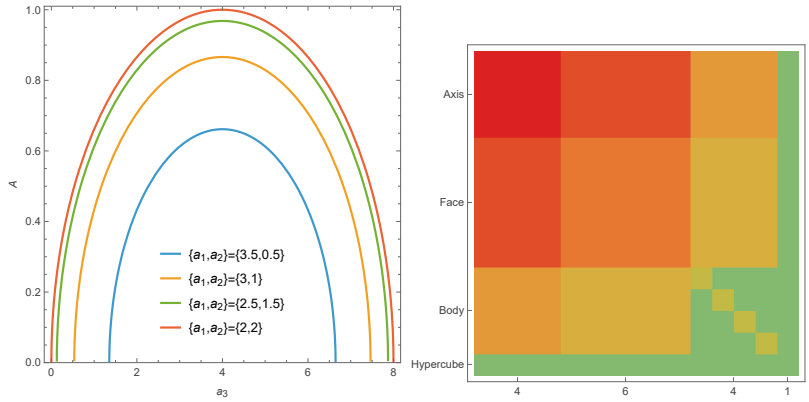

Fig. 2 (a) Heron's formula with two legs fixed: the area of a triangle as a function of the squared third side is stationary exactly where the third side is the hypotenuse of a right triangle, $a_3 = a_1 + a_2$. Every triangle containing the hypercube diagonal has legs of squared lengths $(2, 2)$ or $(1, 3)$; both curves are flat at $a_3 = 4$, which is Theorem 3.1. (b) The block structure of the symbol $\mathsf{M}(k)$ on the 15 edge classes, ordered 4 axes, 6 face diagonals, 4 body diagonals, 1 hypercube diagonal. The hypercube row and column vanish identically; the body-diagonal block is the constant $-\frac{1}{2}I_4$ with no mutual off-diagonal entries; the body strains still couple to axes and face strains.

we refer to this as the "reduced symbol" on $x = \mathrm{vec}_F\, h$. Set $D_Q = Q^{\mathsf{T}}\mathsf{M}'Q$. Consider the lemma:

Lemma 3.3 (faithful elimination)**.** *Let* M' *be the interacting symbol and let* $S \in \mathbb{C}^{14\times 10}$ *and* $Z \in \mathbb{C}^{14\times 4}$ *such that* $[S\ Z]$ *and* $Z^{\mathsf{T}}\mathsf{M}'Z$ *are invertible. Write* $\Sigma = S^{\mathsf{T}}\mathsf{M}'S - S^{\mathsf{T}}\mathsf{M}'Z(Z^{\mathsf{T}}\mathsf{M}'Z)^{-1}Z^{\mathsf{T}}\mathsf{M}'S$*. Then*

$$x \longmapsto Sx - Z(Z^{\mathsf{T}}\mathsf{M}'Z)^{-1}Z^{\mathsf{T}}\mathsf{M}'Sx$$

is an isomorphism from $\ker\Sigma$ *onto* $\ker\mathsf{M}'$*. The two kernels have equal dimension, although their vectors live in different spaces.*

Proof Write $J = [S\ Z]$. Every $c \in \mathbb{C}^{14}$ is uniquely $c = Sx + Z\beta$. Since J is invertible, $\mathsf{M}'c = 0$ if and only if $J^{\mathsf{T}}\mathsf{M}'c = 0$. Partitioning that product gives the pair

$$Z^{\mathsf{T}}\mathsf{M}'Sx + (Z^{\mathsf{T}}\mathsf{M}'Z)\beta = 0, \qquad S^{\mathsf{T}}\mathsf{M}'Sx + S^{\mathsf{T}}\mathsf{M}'Z\beta = 0. \tag{15}$$

The first block is invertible by hypothesis, so $\beta = -(Z^{\mathsf{T}}\mathsf{M}'Z)^{-1}Z^{\mathsf{T}}\mathsf{M}'Sx$. Substituting into the second block is $\Sigma x = 0$, and the resulting c is the displayed map. Conversely, every null vector of M' arises in this way from a unique x. Thus the map is a linear bijection $\ker\Sigma \to \ker\mathsf{M}'$. □

Then Lemma 3.3 means that if D_Q is invertible,

$$x \longmapsto c = Px - QD_Q^{-1}Q^{\mathsf{T}}\mathsf{M}'Px \tag{16}$$

is a bijection from $\ker\mathsf{E}$ to $\ker\mathsf{M}'$. The Q equation fixes the eliminated coordinates, and the remaining equation is $\mathsf{E}x = 0$.

Expand $\mathsf{E}(u) = \mathsf{E}_2(u) + \mathsf{E}_4(u) + \dots$ in homogeneous polynomials in $u \in \mathbb{C}^4$; odd orders vanish by Lemma 2.2(i).

Theorem 3.4 (isotropic quadratic sector)**.** *As polynomials in $u \in \mathbb{C}^4$,*

$$\mathsf{E}_2(u)\,\mathrm{vec}_F\, h = -\tfrac{1}{4}\,\mathrm{vec}_F(G(u)h), \tag{17}$$

$$G(u)h = (u\cdot u)h - u(hu)^{\mathsf{T}} - (hu)u^{\mathsf{T}} + (u\otimes u)\,\mathrm{tr}\,h \tag{18}$$

$$+\,\delta\big(u^{\mathsf{T}}hu - (u\cdot u)\,\mathrm{tr}\,h\big). \tag{19}$$

G the linearized Einstein operator in Fourier space (2 times the Fourier transform of the linearized Einstein tensor). Here δ is the Euclidean identity tensor, and $u\cdot u$ is the complex bilinear extension of the Euclidean form. For real nonzero u this says $\mathsf{E}_2(u)$ has eigenvalues

$$\begin{aligned} -\tfrac{1}{4}|u|^2 &\quad \textit{with multiplicity 5, on Euclidean transverse traceless } h,\\ 0 &\quad \textit{with multiplicity 4, on gauge } h = u\otimes\xi + \xi\otimes u,\\ +\tfrac{1}{2}|u|^2 &\quad \textit{with multiplicity 1, on the transverse trace,} \end{aligned}$$

where transverse means $h_{\mu\nu}u^\nu = 0$: these are the eigenvalues of the quadratic operator of $\frac{1}{2}\int R\sqrt{g}$, Regge's normalization of the Einstein action, in the same coordinates. These five Euclidean TT directions are off-shell tensor components, not five propagating gravitons. Two physical polarizations remain after the complex characteristic equation and the gauge quotient are imposed. The negative TT sign is the sign of the stated Einstein action; equality of characteristic sets with a scalar Laplacian does not make the metric quadratic form a positive scalar energy.

Proof The identity has two parts: the quadratic reduced symbol does not see the four non-metric directions, and the remaining 10×10 matrix of quadratic forms equals $-\frac{1}{4}G$. Expand $\mathsf{M}'(su) = \mathsf{M}'_0 + s^2\mathsf{M}'_2(u) + s^4\mathsf{M}'_4(u) + \cdots$ in homogeneous polynomials in s. Odd orders vanish because M' is a cosine polynomial (Lemma 2.2(i)). The image of P lies in $\ker\mathsf{M}'_0$, so $P^{\mathsf{T}}\mathsf{M}'_0 = 0$. The cross block of the Schur formula therefore has no zeroth order terms in s,

$$P^{\mathsf{T}}\mathsf{M}'(su)\,Q = s^2 P^{\mathsf{T}}\mathsf{M}'_2(u)\,Q + O(s^4).$$

The block $Q^{\mathsf{T}}\mathsf{M}'_0Q$ is invertible (eigenvalues $-8,-2,-2,-2$). The lowest order term in the Schur correction $P^{\mathsf{T}}\mathsf{M}'Q\,(Q^{\mathsf{T}}\mathsf{M}'Q)^{-1}Q^{\mathsf{T}}\mathsf{M}'P$ in (14) is a product of two factors of order s^2 (the lowest order terms of $P^{\mathsf{T}}\mathsf{M}'(su)\,Q$ and $Q^{\mathsf{T}}\mathsf{M}'P$) and a zeroth order term $(Q^{\mathsf{T}}\mathsf{M}'_0Q)^{-1}$ so the entire Schur correction is $O(s^4)$. Hence

$$\mathsf{E}_2(u) = P^{\mathsf{T}}\mathsf{M}'_2(u)\,P.$$

Both sides of (18) are then 10×10 matrices of quadratic forms in u. Their coefficients are rational in unnormalized tensor coordinates; the Frobenius rescaling is a fixed congruence. The equality is a finite identity of rational polynomials; expanding both sides in exact arithmetic gives the zero matrix (Appendix B). The same matrices agree to 10^{-40} at twelve random complex u in forty-digit arithmetic. □

The three eigenvalues of G can be evaluated from (19).

1. For transverse traceless h, $\operatorname{tr} h = 0$ and $hu = 0$ so $Gh = (u \cdot u)h$.
2. For the transverse trace $P_\perp = \delta - uu^{\mathsf{T}}/(u \cdot u)$, we still have $hu = 0$ so $GP_\perp = (u \cdot u)P_\perp - (u \cdot u)\delta \operatorname{tr} P_\perp + uu^T \operatorname{tr} P_\perp$. In order for this to be an eigenvector, $-(u \cdot u)\delta \operatorname{tr} P_\perp + uu^T \operatorname{tr} P_\perp = cP_\perp$, where c is some constant, but inputting the definition of $P_\perp$ and the fact that $\operatorname{tr} P_\perp = 3$ gives

$$-3(u \cdot u)\delta + 3uu^{\mathsf{T}} = c(\delta - uu^{\mathsf{T}}/(u \cdot u)) \tag{20}$$

   from which we see $c = -3u \cdot u$ and therefore $GP_\perp = -2(u \cdot u)P_\perp$.
3. $Gh = 0$ for $h = u \otimes \xi + \xi \otimes u$ can be verified by choosing an arbitrary component u and ξ and direct algebraic reduction, though it is lengthy.

3.2.1 Connection to continuum case

Following the presentation in [10, 14], we rewrite the weak field continuum Lagrangian

$$L = \frac{1}{2}\partial_\lambda h^{\lambda\mu}(\partial_\nu h^\nu_\mu - \partial_\mu h^\nu_\nu) + \frac{1}{4}\partial_\lambda h^\mu_\mu \partial^\lambda h^\nu_\nu - \frac{1}{4}\partial_\lambda h_{\mu\nu}\partial^\lambda h^{\mu\nu} \tag{21}$$

as

$$L = -\frac{1}{2}\partial_\lambda h_{\alpha\beta} V^{\alpha\beta\mu\nu}\partial^\lambda h_{\mu\nu} + \frac{1}{2}C_\mu C^\mu \tag{22}$$

where

$$V^{\alpha\beta\mu\nu} = \frac{1}{2}\delta^{\alpha\mu}\delta^{\beta\nu} - \frac{1}{4}\delta^{\alpha\beta}\delta^{\mu\nu} \tag{23}$$

$$C_\mu = \partial_\nu h^\nu_\mu - \frac{1}{2}\partial_\mu h^\nu_\nu \tag{24}$$

are the continuum forms in [10], Appendix D, and [14], equations (144)–(149). The density is quadratic in the field. Its bilinear Fourier kernel, the same convention as Remark 2.3, puts momentum u on one factor and $-u$ on the other, i.e. $h_{\mu\nu}(r) = e^{\pm \mathrm{i}u\cdot r}H_{\mu\nu}$ with $H_{\mu\nu}$ being a constant polarization tensor. The derivatives in the V term contribute $(\mathrm{i}u)(-\mathrm{i}u) = u \cdot u$, while $C_\mu(u)C^\mu(-u) = (C_1 x)\cdot(C_1 x)$ with $x = \operatorname{vec}_F H$ and $C_1(u)$ the 4×10 matrix $(C_1 x)_\nu = u^\mu H_{\mu\nu} - \frac{1}{2}u_\nu \operatorname{tr} H$. Since the Regge action is half the Einstein–Hilbert action in this normalization, its quadratic action is $\frac{1}{2}x^{\mathsf{T}}\mathsf{E}_2 x$. The corresponding Hessian satisfies

$$x^{\mathsf{T}}\mathsf{E}_2(u)\,x = \tfrac{1}{2}\big[-(u \cdot u)\,H_{\alpha\beta}V^{\alpha\beta\mu\nu}H_{\mu\nu} + (C_1 x)\cdot(C_1 x)\big]. \tag{25}$$

For a real unit wave vector u, the Hessian eigenvalue equation is

$$\mathsf{E}_2(u)x = \lambda x. \tag{26}$$

Ensuring that $h_{\mu\nu}$ is transverse traceless $h^\alpha_\alpha = h_{\mu\nu}u^\mu = 0$ sets five components of x in terms of the other five, so there are five linearly independent vectors in the 10D space. Inputting a generic transverse traceless h and reducing shows the eigenvalue is $\lambda_{TT} = -1/4$. For each u, there is a single transverse trace $\operatorname{vec}_F(P_\perp)$, and the eigenvalue

$\lambda_\perp = 1/2$ can again be deduced by algebraic reduction. Finally, there are four linearly independent 4D vectors ξ, so there are four independent $\mathrm{vec}_F(u_\mu\xi_\nu + \xi_\mu u_\nu)$, and the eigenvalues come out to $\lambda_G = 0$. Table 3 shows the calculated spectrum of E_2 on six real directions for u. The calculated values agree with the expected continuum values.

Direction $u/\lvert u\rvert$	TT eigenvalues ($\times 5$)	gauge ($\times 4$)	trace
$(1,0,0,0)$	-0.25	$< 2 \times 10^{-42}$	0.5
$(1,1,0,0)/\sqrt{2}$	-0.25	$< 9 \times 10^{-42}$	0.5
$(1,1,1,0)/\sqrt{3}$	-0.25	$< 1 \times 10^{-41}$	0.5
$(1,1,1,1)/2$	-0.25	$< 8 \times 10^{-42}$	0.5
$(1,2,3,4)/\sqrt{30}$	-0.25	$< 4 \times 10^{-41}$	0.5
$(3,-1,2,0)/\sqrt{14}$	-0.25	$< 9 \times 10^{-42}$	0.5

Table 3 Spectrum of $\mathsf{E}_2(u)$ at unit $\lvert u\rvert$, forty-digit arithmetic. The TT eigenvalue is -0.25 to 1.1×10^{-41} on every direction.

Remark 3.5 (the quartic part is not isotropic off the cone). The quartic part $\mathsf{E}_4(u)$ restricted to the five TT polarizations of a real direction is not a multiple of the identity. The exact spectra of the restricted quartic form are

$$u = (1,0,0,0): \quad \frac{11}{384}\ (2), \quad \frac{31}{768}\ (1), \quad \frac{1}{192}\ (2),$$
$$u = (1,1,0,0)/\sqrt{2}: \quad \frac{1}{24}\ (2), \quad \frac{1}{192}\ (1), \quad \frac{13}{384}\ (1), \quad \frac{1}{96}\ (1),$$

where parentheses give multiplicities. These are eigenvalues of the five-dimensional TT restriction. They are obtained from $P^{\mathsf{T}}(\mathsf{M}'_4 - \mathsf{M}'_2\mathsf{M}'^{+}_0\mathsf{M}'_2)P$, where the inverse on the non-metric subspace is $\mathsf{M}'^{+}_0 = 21\mathsf{M}'_0/64 + 5(\mathsf{M}'_0)^2/128$. In particular, diagonal evaluations on selected TT tensors need not be eigenvalues when the form has off-diagonal entries. The polarization dependence at quartic order is real. What Section 4 shows is that it disappears exactly on the propagating branch: the combination of E_4 with the second-order correction from E_2 that governs the dispersion is proportional to the identity on the two physical polarizations.

4 The transverse-traceless branch is the Laplacian branch

The question is a kernel count. Four null vectors of $\mathsf{M}'(k)$ come from moving vertices and carry no physical content. A propagating polarization is a null vector beyond those four. This section counts the kernel at every complex k, exactly, by changing coordinates on the ten edge classes that remain once the body diagonals have been eliminated. The new coordinates are the trace-reversed metric perturbation, and in them the symbol becomes the continuum weak-field operator of Section 3 with each

derivative replaced by a single lattice difference. Every statement here is an identity of complex bilinear forms; no time direction is chosen until Section 5.

Write $z_i = e^{\mathrm{i}k_i}$, $f_i = z_i - 1$, and $t_i = 1 - z_i^{-1}$, for $i = 1, \ldots, 4$. All z_i are nonzero, even when k is complex. For a matrix-valued function define $X^\sharp(k) = X(-k)^{\mathsf{T}}$; this equals the Hermitian adjoint for real k when the coefficients are real. The scalar lattice symbol is

$$\mathcal{L}(k) = \sum_i (2 - z_i - z_i^{-1}) = -\sum_i f_i t_i. \tag{27}$$

It is worth reducing this into a form we will use later. Converting the exponential form of z_i to trigonometric form gives $\mathcal{L}(k) = \sum_i 2(1 - \cos(k_i))$, using the double angle and Pythagorean identities gives

$$\mathcal{L}(k) = \sum_i 4\sin^2(\frac{k_i}{2}). \tag{28}$$

4.1 Ten coordinates and four constraints

For this section use the vertex convention $\mathrm{d}a_{(D,x)} = c_D e^{\mathrm{i}k\cdot x}$. It is related to the midpoint convention by

$$\mathsf{M}_{\text{vert}} = \Phi \mathsf{M}_{\text{mid}} \Phi^\sharp, \qquad \Phi = \operatorname{diag}(e^{\mathrm{i}k\cdot D/2}). \tag{29}$$

The phases are nonzero for every complex k, so this congruence preserves nullity.

We previously considered reducing $\mathsf{M}' \to \mathsf{E}$, where E is in terms of the metric strains. Another helpful reduction is $\mathsf{M}' \to \mathsf{R}$, which eliminates the body diagonal block $-1/2 I_4$. Recall P was the map between the 10D metric strain space $\mathcal{M}$ and the 14D squared interacting edge deformation space $\mathcal{A}'$ and Q was the map between the 4D complement and the $\mathcal{A}'$. Now let N be a map between $\mathcal{A}'$ and the 10D axis and face diagonal space $\mathcal{A}_{af}$, and let O be the map between $\mathcal{A}'$ and the 4D space spanned by only the body diagonals $\mathcal{A}_{bd}$. Then define

$$\mathsf{R} = N^T \mathsf{M}' N - N^T \mathsf{M}' O (O^T \mathsf{M}' O)^{-1} O^T \mathsf{M}' N \tag{30}$$

Because the M' block on the interacting body diagonals is $-\frac{1}{2} I_4$ in our convention, $O^T \mathsf{M}' O$ is trivially invertible (unlike $Q^T \mathsf{M}' Q$), and $(O^T \mathsf{M}' O)^{-1} = -2 I_4$. Using the $\sharp$ symmetry of M' allows us to write

$$\mathsf{R} = N^T \mathsf{M}' N + 2\mathsf{B}^\sharp \mathsf{B} \tag{31}$$

where $\mathsf{B} = O^T \mathsf{M}' N$ is a 4×10 matrix.

In studies of gravitational waves in the weak field continuum case, it is frequently convenient to work in terms of the trace-reversed perturbations (see e.g. [17, 18]), which can be written as the following in our case:

$$\bar{h}_{\mu\nu} = h_{\mu\nu} - \frac{1}{2}\delta_{\mu\nu} h^\lambda_\lambda. \tag{32}$$

The matrix $\beta = I_4 - \frac{1}{2}J_4$, where every entry of J_4 is one, gives the action of the trace reverse operation on the diagonal elements of a symmetric 4×4 tensor, i.e.

$$\beta \begin{pmatrix} h_{11} \\ h_{22} \\ h_{33} \\ h_{44} \end{pmatrix} = \begin{pmatrix} \bar{h}_{11} \\ \bar{h}_{22} \\ \bar{h}_{33} \\ \bar{h}_{44} \end{pmatrix} \tag{33}$$

The off diagonal terms $\mu \neq \nu$ are unaltered by the trace reverse operation.

Recall the definitions from remark 2.3 and consider

$$y = \mathrm{vec}_P(\bar{h}) \tag{34}$$

so $y_{\mu\nu} = \bar{h}_{\mu\nu}$, and we write y_i for y_{ii}. These are the variables of [14], equation (148). The constant matrix

$$\mathsf{V} = \mathrm{diag}(\beta/2,\, I_6) \tag{35}$$

satisfies, for every real symmetric h,

$$y^{\mathsf{T}}\mathsf{V}\, y = \tfrac{1}{2}h^{\mu\nu}h_{\mu\nu} - \tfrac{1}{4}(\mathrm{tr}\, h)^2 = h_{\alpha\beta}V^{\alpha\beta\mu\nu}h_{\mu\nu}, \tag{36}$$

which is (23) written in these coordinates ([14], equations (146) and (149)). Because $\beta^2 = I_4$, V is invertible with $\mathsf{V}^{-1} = \mathrm{diag}(2\beta, I_6)$.

Write $X \in \mathcal{A}_{\mathrm{af}}$ for the squared-length amplitudes of the four axis and six face classes. The change of coordinates $\mathsf{W}(k) : \mathcal{M} \to \mathcal{A}_{\mathrm{af}}$ is $X = \mathsf{W}(k)y$ with

$$X_i = z_i(\beta y)_i, \qquad\qquad X_{ij} = 2y_{ij} - z_i z_j \sum_{r \notin \{i,j\}} y_r. \tag{37}$$

At $k = 0$ this is the metric strain map of Section 2: β restores the diagonal components $h_{\mu\mu}$ from the trace-reversed ones, and (37) reduces to $\mathrm{d}a_D = D^{\mathsf{T}}hD$. The factors z_i and $z_i z_j$ are the phase of the far end of the edge. They multiply the diagonal part only, and that asymmetry is what gives the constraint (41) a forward difference in its own index and backward differences in the others. The matrix W has a block structure

$$\mathsf{W} = \begin{pmatrix} \mathrm{diag}(z_i)\beta & 0_{4\times 6} \\ \Gamma_{6\times 4} & 2I_6 \end{pmatrix} \tag{38}$$

where Γ has components assigned as follows:

$$\text{for row } (ij), \begin{cases} 0 & \text{if column} \in \{i,j\} \\ -z_i z_j & \text{if column} \notin \{i,j\} \end{cases}. \tag{39}$$

In any event, the block structure means Γ is irrelevant to the determinant, so using $\det \beta = -1$,

$$\det \mathsf{W} = -64\, z_1 z_2 z_3 z_4 \neq 0. \tag{40}$$

Every entry in W is a polynomial in the nonzero z_i, and it is an invertible change of coordinates at every complex k (nonzero determinant). Define $\mathsf{C}(k) : \mathcal{M} \to \mathcal{G}$ by

$$(\mathsf{C}y)_i = f_i\, y_{ii} + \sum_{j \neq i} t_j\, y_{ij}. \tag{41}$$

In the ordering of Remark 2.3, this is the 4×10 block matrix

$$\mathsf{C} = \big[\, F \mid S \,\big], \qquad F = \operatorname{diag}(f_i), \qquad S_{i,\{p,q\}} = \begin{cases} t_q, & i = p, \\ t_p, & i = q, \\ 0, & i \notin \{p, q\}, \end{cases} \tag{42}$$

with face columns ordered as $\{1,2\}, \{1,3\}, \{1,4\}, \{2,3\}, \{2,4\}, \{3,4\}$. Explicitly,

$$S = \begin{pmatrix} t_2 & t_3 & t_4 & 0 & 0 & 0 \\ t_1 & 0 & 0 & t_3 & t_4 & 0 \\ 0 & t_1 & 0 & t_2 & 0 & t_4 \\ 0 & 0 & t_1 & 0 & t_2 & t_3 \end{pmatrix}. \tag{43}$$

This is a single lattice divergence of y on its first index, forward in the repeated index and backward in the others; as $k \to 0$ it becomes $ik^\mu \bar{h}_{\mu i}$, which is the de Donder vector C_μ from (24) with the plane wave perturbation; its matrix is given in [14], equation (142). The exact weak-field factorization is

$$\mathsf{W}^\sharp \mathsf{R}\, \mathsf{W} = -\tfrac{1}{2}\, \mathsf{K}(k), \qquad \mathsf{K}(k) = \mathcal{L}(k)\, \mathsf{V} - \mathsf{C}^\sharp(k)\, \mathsf{C}(k). \tag{44}$$

Read against Theorem 3.4: the quadratic sector was the continuum Einstein operator to leading order in k, and (44) is the same operator with $|k|^2$ replaced by $\mathcal{L}(k)$ and each derivative by one lattice difference, with no correction at any order in k. Equation (44) is verified as an identity, not sampled. Substituting the 302 rational coupling weights into R and forming $\mathsf{W}^\sharp \mathsf{R} \mathsf{W} + \frac{1}{2}\mathsf{K}$ gives zero in all 100 entries as rational functions of $z_1, \ldots, z_4$ (Appendix B).

Lemma 4.1 (the constraint and the gauge modes)**.** *Let $k \in \mathbb{C}^4 \setminus 2\pi\mathbb{Z}^4$. Then*

1. *$\mathsf{C}(k)$ and $\mathsf{C}(-k)$ both have rank 4;*
2. *$\mathsf{C}\, \mathsf{V}^{-1} \mathsf{C}^\sharp = \mathcal{L}\, I_4$, and hence $\mathsf{K}\, \mathsf{V}^{-1} \mathsf{C}^\sharp = 0$;*
3. *the four columns of $\mathsf{V}^{-1}\mathsf{C}^\sharp$ are the vertex displacement modes: the displacement ξ of Lemma 2.2(iii) has $y = -\mathsf{V}^{-1}\mathsf{C}^\sharp \xi$, and these four modes are independent.*

Proof (i) The hypothesis $k \notin 2\pi\mathbb{Z}^4$ means some $z_i \neq 1$, hence some $f_i \neq 0$. A row vector b^T lies in the left kernel of C if and only if $b^\mathsf{T} F = 0$ and $b^\mathsf{T} S = 0$. The first is $b_i f_i = 0$ for each i, so $b_i = 0$ whenever $f_i \neq 0$; fix one such index i. The $\{i,j\}$ column of S then gives $b_i t_j + b_j t_i = b_j t_i = 0$. But $t_i = f_i / z_i \neq 0$, so $b_j = 0$ for every j, including those with $f_j = 0$. Hence $b = 0$ is the only null vector, so $\mathsf{C}(k)$ has rank 4. The same argument with

$F(-k) = -\operatorname{diag}(t_i)$ and with the columns of $S(-k)$ equal to $-f_j e_i - f_i e_j$ shows that $\mathsf{C}(-k)$ has rank 4.

(ii) Using the above forms of $\mathsf{C}, \mathsf{C}^\sharp, \mathsf{V}^{-1}$ and multiplying gives $\mathsf{C}\mathsf{V}^{-1}\mathsf{C}^\sharp = \big(8 - \sum_{j=1}^{4}(e^{\mathrm{i}k_j} + e^{-\mathrm{i}k_j})\big) I_4$, from (27) the prefactor is $\mathcal{L}(k)$. Then

$$\mathsf{K}\mathsf{V}^{-1}\mathsf{C}^\sharp = (\mathcal{L}(k)\mathsf{V} - \mathsf{C}^\sharp\mathsf{C})\mathsf{V}^{-1}\mathsf{C}^\sharp = \mathcal{L}(k)\mathsf{V}\mathsf{V}^{-1}\mathsf{C}^\sharp - \mathsf{C}^\sharp(\mathsf{C}\mathsf{V}^{-1}\mathsf{C}^\sharp) = \mathcal{L}(k) I_{10}\mathsf{C}^\sharp - \mathsf{C}^\sharp\mathcal{L}(k) I_4 = 0. \tag{45}$$

(iii) In blocks, $F^\sharp\xi = -\operatorname{diag}(t_i)\xi$ and $(S^\sharp\xi)_{\{i,j\}} = -f_j\xi_i - f_i\xi_j$. Displacing every vertex by $\xi e^{\mathrm{i}k\cdot x}$ changes the squared lengths of the axis and face classes by $X_i = 2f_i\xi_i$ and $X_{ij} = 2(z_i z_j - 1)(\xi_i + \xi_j)$, which is Lemma 2.2(iii) in the vertex convention. Solving (37) for y is the same as $y = -\mathsf{V}^{-1}\mathsf{C}^\sharp\xi$. Injectivity of $\xi \mapsto \mathsf{V}^{-1}\mathsf{C}^\sharp\xi$ is satisfied iff $\operatorname{rank}\mathsf{C}^\sharp(k) = 4$. But $\mathsf{C}^\sharp(k) = \mathsf{C}(-k)^{\mathsf{T}}$, so (i) guarantees $\operatorname{rank}\mathsf{C}^\sharp(k) = 4$. □

Theorem 4.2 (exact branch)**.** *For every $k \in \mathbb{C}^4 \setminus 2\pi\mathbb{Z}^4$, the interacting fourteen-dimensional symbol satisfies*

$$\dim\ker\mathsf{M}'(k) = \begin{cases} 4, & \mathcal{L}(k) \neq 0, \\ 6, & \mathcal{L}(k) = 0. \end{cases} \tag{46}$$

Its null space modulo the four vertex-displacement modes therefore has dimension zero off $\mathcal{L} = 0$ and dimension two on $\mathcal{L} = 0$. The reduced metric symbol $\mathsf{E}(k)$ has the same nullity wherever its non-metric block is invertible.

Proof Eliminating the invertible body block preserves nullity, as does the invertible change W. If $\mathcal{L} \neq 0$ and $\mathsf{K}y = 0$, then $y = \mathcal{L}^{-1}\mathsf{V}^{-1}\mathsf{C}^\sharp\mathsf{C}y$. Every null vector therefore lies in the four-dimensional image of $\mathsf{V}^{-1}\mathsf{C}^\sharp$. Lemma 4.1 shows that this whole image is the kernel, giving nullity four. If $\mathcal{L} = 0$, then $\mathsf{K} = -\mathsf{C}^\sharp\mathsf{C}$. The map C is surjective and $\mathsf{C}^\sharp$ is injective, both of rank four, so their product has rank four and K has nullity six. □

The two extra null vectors on $\mathcal{L} = 0$ occur at the same wave vectors, so there is a single branch: no massive companion, no second massless branch, no birefringence in this linearized symbol. For real k the sum $\mathcal{L}(k) = \sum_\mu 4\sin^2(k_\mu/2)$ vanishes only on $2\pi\mathbb{Z}^4$, which the theorem excludes as the uniform mode of Proposition 3.2 and its periodic images; the branch is therefore reached only by continuing k into the complex zone, which is what Section 5 does. Since $\mathcal{L}$ is even in each k_μ separately, the branch carries the full hyperoctahedral group of order 384, while the triangulation has only the subgroup of order 48 in Lemma 2.2(ii): the cone is more symmetric than the lattice carrying it. Table 4 checks the count directly in the edge variables, without W.

5 Time continuation of the Euclidean symbol

The Euclidean characteristic function is entire in momentum. Choose a real unit vector T and a real unit vector $\hat{n} \perp T$, and set $u = \mathrm{i}\omega T + \mathrm{k}\hat{n}$. The equation $\mathcal{L}(\mathrm{i}\omega T + \mathrm{k}\hat{n}) = 0$ defines the continuation studied here. The propagation speed in the infrared limit is set to one; comparison with the speed of light requires a photon dispersion law.

This substitution continues the Euclidean symbol. A direct Lorentzian Regge calculation instead changes the squared edge lengths, areas and angle derivatives before forming the Hessian. Section 6 performs that construction on $g_L = I_4 - J_4$. Its axis edges are null, but its higher-dimensional simplices and hinges are nondegenerate. Both constructions here concern the quadratic action about their stated flat backgrounds.

5.1 Time along an axis

Theorem 5.1. *Let $T = e_4$, $\mathrm{k} \geq 0$, and $\hat{n} = (n_1, n_2, n_3, 0)$ be a unit vector. The TT branch is*

$$\omega(\mathrm{k}, \hat{n}) = 2\,\mathrm{arcsinh}\sqrt{\sum_{j=1}^{3} \sin^2 \frac{\mathrm{k}n_j}{2}}, \tag{47}$$

the nonnegative real-frequency branch, bounded by $2\,\mathrm{arcsinh}\sqrt{3} \simeq 2.634$. Its expansion is

$$\omega = \mathrm{k}\Big(1 - \frac{1 + A(\hat{n})}{24}\mathrm{k}^2 + O(\mathrm{k}^4)\Big), \qquad A(\hat{n}) = \sum_{j=1}^{3} n_j^4, \tag{48}$$

so the phase velocity is $1 - \kappa\mathrm{k}^2 + O(\mathrm{k}^4)$ and the radial group velocity is $1 - 3\kappa\mathrm{k}^2 + O(\mathrm{k}^4)$ with

$$\kappa(\hat{n}) = \frac{1 + A(\hat{n})}{24} \in \Big[\frac{1}{18}, \frac{1}{12}\Big], \tag{49}$$

$\kappa = 1/12$ on an axis, $1/16$ on a face diagonal, $1/18$ on a body diagonal, and the direction average over the sphere is $1/15$. Both polarizations obey (47): there is no birefringence at any order.

Proof Take the form (28) in $\mathcal{L}(u) = 0$ with $u_4 = \mathrm{i}\omega$. The complex function identity $\sin^2(\mathrm{i}\omega/2) = -\sinh^2(\omega/2)$ allows us to conclude

$$4\sinh^2(\omega/2) = \sum_{j=1}^{3} 4\sin^2(\mathrm{k}n_j/2). \tag{50}$$

Solving for ω gives (47). The frequency bound uses $\sum_j \sin^2 \leq 3$. The phase and group velocities follow immediately from definitions $v_{ph} = \omega/\mathrm{k}$, $v_{gr} = \frac{d\omega}{d\mathrm{k}}$ and (48). The range of κ can be determined with constrained optimization: $O(n_1, n_2, n_3, \lambda) = \sum_{j=1}^{3} n_j^4 + \lambda(1 - \sum_{j=1}^{3} n_j^2)$, then evaluating κ on the resulting $\nabla O = 0$ set. This set corresponds to axes, faces, and body diagonals of 3D cubes.

A can be written in polar form as

$$A(\theta, \phi) = \sin^4(\theta)(\sin^4(\phi) + \cos^4(\phi)) + \cos^4(\theta). \tag{51}$$

then the average over the sphere is given by $1/(4\pi)\int A(\theta, \phi)\sin(\theta)d\theta d\phi$. □

For the exact speed bounds, define the abbreviations $p_j = \mathrm{k}n_j$ and $S = \sum_j \sin^2(p_j/2)$. Then

$$\omega = 2\,\mathrm{arcsinh}\sqrt{S} < 2\sqrt{S} \leq |p| \qquad (p \neq 0 \text{ in the spatial zone}). \tag{52}$$

The group velocity is the vector $\nabla_p \omega$, generally not parallel to p in an anisotropic medium. Direct differentiation gives

$$(v_g)_j = \frac{\sin p_j}{2\sqrt{S}\sqrt{1+S}}, \qquad |v_g|^2 = \frac{S - \sum_j \sin^4(p_j/2)}{S(1+S)} < 1 \quad (S > 0). \tag{53}$$

Both speeds approach one as $\mathrm{k} \to 0$, as can be inferred from the small k expansions calculated in Theorem 5.1.

Figure 4 shows κ over the sphere of directions; Figure 5 the full branch along an axis and a body diagonal; Figure 3 the curves of constant frequency in a coordinate plane of wave vectors. At long wavelength these are the continuum circles $\mathrm{k} = \omega$; toward the zone edge they become a diamond with its vertices on the axes, lying outside the circle of the same frequency because the wave is slower, and departing from it most along the axes, where κ is largest.

The same three pictures describe the simplest lattice field. A scalar ϕ on $\mathbb{Z}^4$ with action $\frac{1}{2}\sum_{x,\mu}(\phi(x+e_\mu)-\phi(x))^2$ has symbol $\mathcal{L}(k)$, and with the fourth axis as time its dispersion is (47) with the same $\kappa(\hat{n})$. Theorem 4.2 says that the graviton, a rank-two tensor built from fifteen coupled edge fields on a triangulation with forty-eight symmetries, has been given by the Regge action exactly the dispersion of that scalar. When the spacing is sent to zero at fixed wave number, the defect $\kappa \mathrm{k}^2 a^2$ vanishes as a^2 and the continuum graviton is recovered with nothing to tune.

The agreement with the scalar field holds in a stronger sense, and it fixes what the continued frequency means. Call $y \in \mathcal{M}$ *spatial* when $y_4 = y_{14} = y_{24} = y_{34} = 0$, and write $p = (k_1, k_2, k_3)$ for the spatial part of k.

Proposition 5.2 (the spatial transverse-traceless sector)**.** *Let $y \in \mathcal{M}$ be spatial.*

(i) $(\mathsf{C}y)_4 = 0$, *and* $(\mathsf{C}y)_1$, $(\mathsf{C}y)_2$, $(\mathsf{C}y)_3$ *do not involve* z_4.
(ii) If $\mathsf{C}(k)y = 0$ *at one value of* k_4, *then for every* $k_4 \in \mathbb{C}$

$$\mathsf{K}(k)\, y = \mathcal{L}(k)\, \mathsf{V} y, \qquad \textit{hence} \qquad w^{\mathsf{T}} \mathsf{K}(k)\, y = \mathcal{L}(k)\, w^{\mathsf{T}} \mathsf{V} y \quad (w \in \mathcal{M}). \tag{54}$$

(iii) If $(z_1, z_2, z_3) \neq (1,1,1)$, *the spatial* y *with* $\mathsf{C}y = 0$ *and* $y_1 + y_2 + y_3 = 0$ *form a two-dimensional space. On it* $h = \bar{h}$ *and* $y^\dagger \mathsf{V} y = \frac{1}{2}\sum_{\mu,\nu} |h_{\mu\nu}|^2$.
(iv) For real k *with* $S = \sum_{j=1}^{3} \sin^2(\mathrm{k} n_j/2) > 0$, *let* $\omega = 2\,\mathrm{arcsinh}\,\sqrt{S}$. *The function* $G(n) = e^{-\omega|n|}/(2\sinh\omega)$ *on* $n \in \mathbb{Z}$ *satisfies*

$$(2+4S)\, G(n) - G(n+1) - G(n-1) = \delta_{n0}. \tag{55}$$

Proof (i) By (41), $(\mathsf{C}y)_4 = f_4 y_4 + \sum_{j\le 3} t_j y_{j4} = f_4 0 + \sum_{j\le 3} t_j 0 = 0$. For $(\mathsf{C}y)_i$, $i \le 3$, z_4 can only enter through the sum term of (41), but the only summands dependent on z_4 are $t_4 y_{i4} = 0$. (ii) By (i), $\mathsf{C}(k)y$ does not depend on k_4, so if $\mathsf{C}(k)y = 0$ for one k_4 then $\mathsf{C}(k)y = 0$ holds at every k_4. By (44) $\mathsf{K}y = \mathcal{L}\,\mathsf{V}y - \mathsf{C}^\sharp(\mathsf{C}y)$, and the second term drops out. Left multiplying this by w^T and moving past the Laplacian factor (a commuting scalar) recovers the rest.

(iii) Pick any $j \le 3$ such that $z_j \neq 1$ and assign l, m to the values of $\{1,2,3\}$ not already occupied by j. In the columns y_j, y_{jl}, y_{jm} the rows j, l, m of C form a block with determinant $f_j t_j^2 \neq 0$, so the three conditions are independent. The quantity $y_1 + y_2 + y_3 = -\operatorname{tr} h$ for spatial y, and it is not expressible as

$$\sum_i a_i (\mathsf{C}y)_i = \sum_i (a_i f_i y_i) + \sum_{i<l} y_{il}(a_i t_l + a_l t_i) :$$

it requires $a_i f_i = 1$ for each i to recover the diagonal corresponding elements, and the off-diagonal corresponding elements would then need $a_i t_l + a_l t_i = 0$ for each pair. Simultaneously, these give $t_l/f_i + t_i/f_l = 0$ or $t_l f_l + t_i f_i = z_i + z_i^{-1} + z_l + z_l^{-1} - 4 = 0$ for all pairs $i < l$. This would require all $z_j = 1$, which contradicts the hypothesis $z_j \neq 1$. Four independent conditions on six coordinates leaves two dimensions. The condition $y_1 + y_2 + y_3 = -\operatorname{tr} h = 0$ means h is traceless so it equals its trace reversal, and (36) with β acting on a traceless diagonal as the identity gives the form $y^\dagger \mathsf{V} y = \frac{1}{2}\sum_{\mu,\nu} |h_{\mu\nu}|^2$.

(iv) Since $2\cosh\omega = 2 + 4\sinh^2(\omega/2) = 2 + 4S$, the left side is $G(n)\,(2\cosh\omega - e^{\omega} - e^{-\omega}) = 0$ for $n \neq 0$, and $(2\cosh\omega - 2e^{-\omega})/(2\sinh\omega) = 1$ for $n = 0$. □

With time along the fourth axis, the proposition has a direct reading. At fixed real spatial momentum, let the vectors Y_A, Y_B span the two dimensional space of part (iii). They have the scalar symbol $\mathcal{L}(p, k_4) = 4\sin^2(k_4/2) + 4S$. Letting $w^T = Y^\dagger$ and computing $w^T \mathsf{K}(k) Y$ gives $\mathcal{L}(p, k_4) Y^\dagger \mathsf{V} Y$ by part (ii). By part (iii), $Y^\dagger \mathsf{V} Y$ is positive for nonzero perturbation, so any 0 factor came from the Laplacian term, not from being null with respect to V. This is a statement about the behavior of Y and K. From equation (44) the Regge Hessian pulls back to $-1/2\mathsf{K}$. On the branch $\mathcal{L} = 0$ the Y are null vectors of K, but they are not gauge. By Lemma 4.1 an arbitrary gauge vector is $G = -\mathsf{V}^{-1}\mathsf{C}^\sharp \xi$, cancellation of the $14, 24, 34$ components of g_ξ requires

$$\xi = q(-f_1, -f_2, -f_3, f_4) \tag{56}$$

for some constant q. Cancellation of the 4 component of G requires either $q = 0$ (which makes G a zero vector) or

$$0 = 8 - \sum_{i=1}^{4} (z_i + z_i^{-1}), \tag{57}$$

which is the Laplacian by equation (27). However, G is NOT in the space spanned by the Ys, because computing the spatial trace of G obeying (56),(57) gives $G_1 + G_2 + G_3 = -8q + 4q(z_4 + z_4^{-1})$, which is not zero unless k_4 aliases to 0. The Y_A,Y_B vectors spanning the space of (iii) are therefore the two polarizations counted in Theorem 4.2.

For real momentum, $Y^\dagger \mathsf{K} Y = \mathcal{L}\, Y^\dagger \mathsf{V} Y \ge 0$, so (44) makes the Regge Hessian negative on these amplitudes, which is the transverse-traceless sign in Theorem 3.4; the weight e^{-S_E} with S_E a positive multiple of $-\sum_h A_h \delta_h$ reverses it, and reverses the transverse-trace eigenvalue $+\frac{1}{2}$ of that theorem as well.

Multiplying (55) by $e^{-\mathrm{i}k_4 n}$ and summing

$$\sum_n e^{-\mathrm{i}k_4 n}\left((2 + 4S)\, G(n) - G(n+1) - G(n-1)\right) = e^0$$

$$\sum_n 4SG(n)e^{-\mathrm{i}k_4 n} + \sum_n e^{-\mathrm{i}k_4 n}(2G(n) - G(n+1) - G(n-1)) = 1$$

$$4S\tilde{G} + \tilde{G}(2 - e^{ik_4} - e^{-ik_4}) = 1$$

$$\tilde{G} = \frac{1}{4S + 4\sin^2(k_4/2)} \tag{58}$$

shows that the Fourier series of G in k_4 is $1/\mathcal{L}(p, k_4)$, so, for this sign choice, the free correlation of each amplitude between lattice times 0 and n is proportional to $e^{-\omega|n|}$. That decay rate is the energy a transfer matrix assigns to a free scalar of this kind [19]. Axis time, the sign choice, and decay in both time directions fix (47) in this sector. This is the positive free Gaussian on the two TT amplitudes after the stated sign reversal. It does not construct a positive measure or a transfer matrix for the full Euclidean Regge action, whose trace sector has the opposite sign.

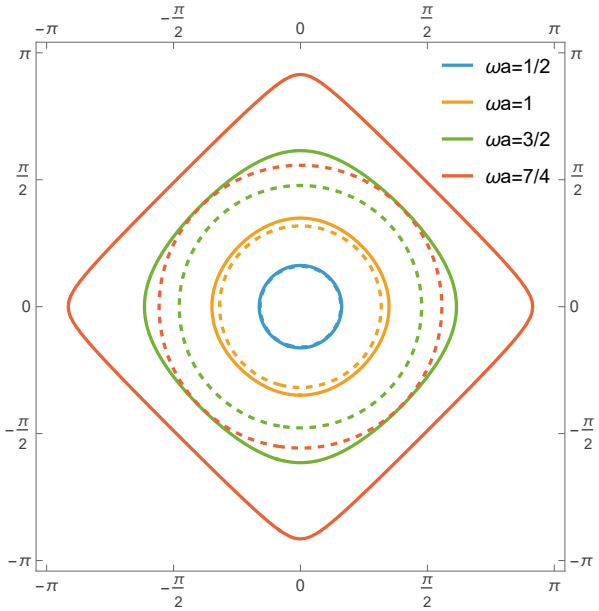

Fig. 3 Curves of constant frequency of the TT branch, $\sin^2(k_1 a/2) + \sin^2(k_2 a/2) = \sinh^2(\omega a/2)$, in the plane $k_3 = 0$ of the Brillouin zone with time along the fourth axis (equation (47)), against the continuum circles of the same frequency. Matching colors identify the same frequency; solid curves are the lattice and dashed curves are the continuum. The lattice curve lies outside the continuum circles everywhere, since the same frequency needs a larger wave number when the wave is slower, and is farthest from it along the axes, where the defect κ is largest. The branch reaches $\omega a = 2\,\mathrm{arcsinh}(1) = 1.763$ at the zone face $k_1 a = \pi$, $k_2 = 0$, and $2\,\mathrm{arcsinh}\sqrt{2} = 2.292$ at the corner.

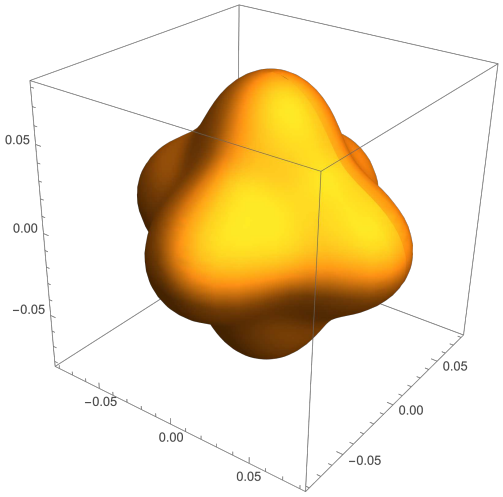

Fig. 4 The anisotropic coefficient $\kappa(\hat{n}) = (1 + \sum_j n_j^4)/24$ of the phase velocity $v_{\mathrm{ph}} = 1 - \kappa \mathrm{k}^2 a^2$, over the sphere of spatial directions, with time along the fourth axis. The defect is largest, 1/12, along the three lattice axes and smallest, 1/18, along the four body diagonals; the face diagonals are saddles at 1/16 and the mean is 1/15. It is positive everywhere, so the wave is slower than the infrared limiting speed in every direction, and it is the same for the two polarizations. In Section 8 this pattern becomes the Standard-Model Extension coefficient $s^{(6)}(\hat{n}) = 2\kappa a^2$.

5.2 Why the anisotropic coefficient is the same for both polarizations

Corollary 5.3 (anisotropy form on the cone)**.** *Let $u = \mathrm{i}T + \hat{n}$ for real orthonormal $T, \hat{n}$. Choose real orthonormal vectors a, b perpendicular to both, and let the columns of U be the Frobenius coordinate vectors of $(aa^{\mathsf{T}} - bb^{\mathsf{T}})/\sqrt{2} \equiv \tau_+$ and $(ab^{\mathsf{T}} + ba^{\mathsf{T}})/\sqrt{2} \equiv \tau_\times$. Then*

$$\Lambda(u) := U^{\mathsf{T}} \mathsf{E}_4(u) U = \frac{1}{48} \left(\sum_{\mu=1}^{4} u_\mu^4 \right) I_2. \tag{59}$$

Proof Write $x = \mathrm{vec}_F\, h$. Let $C_1(u)$ be the 4×10 matrix defined by

$$\big(C_1(u)\, x\big)_\nu = u^\mu h_{\mu\nu} - \tfrac{1}{2} u_\nu \,\mathrm{tr}\, h, \tag{60}$$

so the de Donder vector of (24) is $C = C_1 x$. The continuum quadratic form of Section 3, continued bilinearly, is

$$x^{\mathsf{T}} \mathsf{E}_2(u)\, x = \tfrac{1}{2} \big[-(u \cdot u)\, h_{\alpha\beta} V^{\alpha\beta\mu\nu} h_{\mu\nu} + (C_1 x) \cdot (C_1 x) \big]. \tag{61}$$

On the cone $u \cdot u = 0$, so the V term drops and $\mathsf{E}_2(u) = \frac{1}{2} C_1(u)^{\mathsf{T}} C_1(u)$. The matrix $C_1(u)$ has rank four for $u \neq 0$. Indeed, a left kernel vector $w \in \mathbb{C}^4$ satisfies $w^\nu u^\mu h_{\mu\nu} - \frac{1}{2}(w \cdot u)\,\mathrm{tr}\, h = 0$ for every symmetric h. Equivalently,

$$u w^{\mathsf{T}} + w u^{\mathsf{T}} - (u \cdot w) I_4 = 0. \tag{62}$$

Taking the trace gives $u \cdot w = 0$. Choose i with $u_i \neq 0$. The ii entry then gives $w_i = 0$, and the ij entries give $w_j = 0$ for every j. Thus $w = 0$. Since $C_1(u)^{\mathsf{T}}$ is injective, $\ker \mathsf{E}_2(u) = \ker C_1(u)$

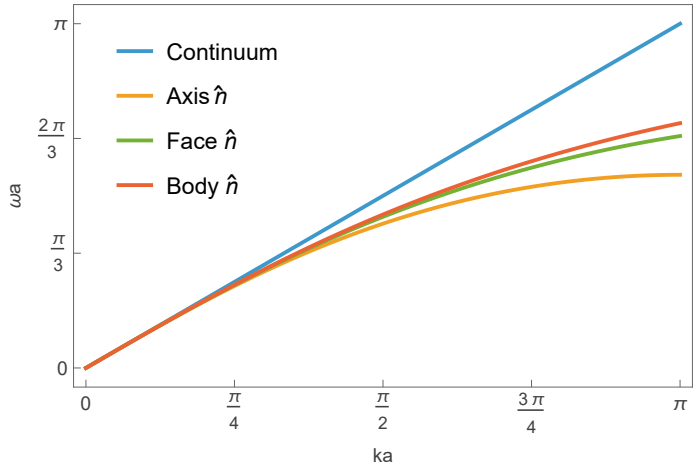

Fig. 5 The exact TT branch with time along an axis, equation (47), and $\hat{n}$ along an axis, face diagonal, or body diagonal, against the continuum cone. The curves lie below the cone for all $\mathrm{k} > 0$. The axis curve reaches $2\,\mathrm{arcsinh}(1) = 1.763$ at $\mathrm{k} = \pi$, its zone edge; along the body diagonal the zone edge is at $\mathrm{k} = \sqrt{3}\,\pi$, beyond the plot, where $\omega = 2\,\mathrm{arcsinh}(\sqrt{3}) \simeq 2.634$.

also over the complex numbers. Thus $N = \ker \mathsf{E}_2(u)$ has dimension six: four gauge directions $h = u \otimes \xi + \xi \otimes u$ and the two columns of U. Move the momentum slightly along $\hat{n}$: $u'(s) = u + s^2 c(s^2)\hat{n}$ and write $v(s) = su'(s) = su + s^3 c\,\hat{n}$. Then

$$\mathcal{L}(v) = v \cdot v - \frac{1}{12} \sum_{\mu} v_\mu^4 + O(s^6), \tag{63}$$

and $u \cdot u = 0$ together with $u \cdot \hat{n} = 1$ give $v \cdot v = 2s^4 c(0) + O(s^6)$ and $\sum_\mu v_\mu^4 = s^4 \sum_\mu u_\mu^4 + O(s^6)$. Hence

$$\mathcal{L}\big(su'(s)\big) = s^4 \Big(2c(0) - \frac{1}{12} \sum_{\mu} u_\mu^4\Big) + O(s^6). \tag{64}$$

The coefficient of s^4 vanishes at $c(0) = \frac{1}{24} \sum_\mu u_\mu^4$. More precisely, $s^{-4}\mathcal{L}(su'(s))$ is an analytic function $\Phi(s^2, c)$ with $\partial_c \Phi(0, c) = 2$, so the implicit function theorem gives an analytic $c(s^2)$ with this value at $s = 0$. In particular $\mathcal{L}(su'(s)) = 0$ for small s. The symbol is even, so

$$s^{-2}\mathsf{E}\big(su'(s)\big) = \mathsf{E}_2(u) + s^2 B + O(s^4), \qquad B = \mathsf{E}_4(u) + c(0)\,\delta_{\hat{n}} \mathsf{E}_2(u). \tag{65}$$

Choose a complement N' to N. The restriction F of the symmetric bilinear form $\mathsf{E}_2(u)$ to N' is nonsingular: a vector of N' that annihilates N' also annihilates N, so it lies in the radical N, and $N \cap N' = 0$. In a basis adapted to $N \oplus N'$,

$$s^{-2}\mathsf{E}\big(su'(s)\big) = \begin{pmatrix} s^2 B_{NN} + O(s^4) & s^2 B_{NN'} + O(s^4) \\ s^2 B_{N'N} + O(s^4) & F + O(s^2) \end{pmatrix}. \tag{66}$$

For small $s \neq 0$ the point $su'(s)$ lies on $\mathcal{L} = 0$ and tends to 0. The block $D_Q = Q^{\mathsf{T}} \mathsf{M}' Q$ in (14) has eigenvalues $-8, -2, -2, -2$ at $k = 0$, as read from (12), and is invertible in a neighborhood of the origin, so it is invertible at $su'(s)$. Lemma 3.3 therefore identifies the kernel of $\mathsf{E}(su'(s))$ with that of $\mathsf{M}'(su'(s))$. Theorem 4.2 makes this kernel six-dimensional, and the 10×10 matrix above has rank four. Its lower block is invertible of rank four, so its Schur complement $s^2 B_{NN} + O(s^4)$ vanishes. At order s^2 this is $B_{NN} = 0$: the bilinear form B vanishes on $N \times N$, and in particular $U^{\mathsf{T}} B U = 0$. The matrix B itself need not vanish on

N; it may map N into the range of $\mathsf{E}_2(u)$. Each column of U is transverse and traceless for every momentum in the plane spanned by T and $\hat{n}$, so $\mathsf{E}_2(v)U = -\frac{1}{4}(v\cdot v)U$. Differentiating at $v = u$ in the direction $\hat{n}$, and using $u\cdot\hat{n} = 1$, gives $U^{\mathsf{T}}\big(\delta_{\hat{n}}\mathsf{E}_2(u)\big)U = -I_2/2$. Therefore

$$0 = U^{\mathsf{T}}BU = \Lambda - c(0)I_2/2, \tag{67}$$

which is the claimed formula. □

The off-shell quartic matrix can distinguish polarizations. Along the characteristic branch its quartic contribution is canceled by the quadratic operator's response to the shifted momentum, identically for both physical polarizations.

5.3 Other lattice directions as time

Theorem 5.4 (lattice directions as time)**.** *Let T be a unit vector along one of the four positive edge-direction classes (axis, face diagonal, body diagonal, hypercube diagonal), and let $\hat{n} \perp T$ be a unit vector. With $u = \mathrm{i}T + \hat{n}$, define $\kappa = \frac{1}{24}\sum_\mu u_\mu^4$ as the analogous coefficient to that defined in Theorem 5.1. Then*

$$24\,\kappa = \sum_\mu \big(n_\mu^4 + T_\mu^4 - 6n_\mu^2 T_\mu^2\big) + 4\mathrm{i}\sum_\mu T_\mu n_\mu\big(n_\mu^2 - T_\mu^2\big), \tag{68}$$

and over the sphere of $\hat{n}$:

- *axis: κ real, $\kappa \in [1/18, 1/12]$;*
- *face diagonal $T = (1,1,0,0)/\sqrt{2}$: κ real, $\kappa \in [-1/12, 1/16]$; for $\hat{n} = (1,-1,0,0)/\sqrt{2}$ it is $-1/12$ and the exact branch $\cosh(\omega/\sqrt{2}) = 1/\cos(\mathrm{k}/\sqrt{2})$ has enhanced speed and is unbounded as $\mathrm{k} \to \pi/\sqrt{2}$;*
- *body diagonal $T = (1,1,1,0)/\sqrt{3}$: $\operatorname{Im}\kappa = \frac{\sqrt{3}}{6}\,n_1n_2n_3$, nonzero unless some $n_j = 0$, with $|\operatorname{Im}\kappa| \le \sqrt{2}/36 = 0.0393$, attained at $\hat{n} = (1,1,-2,0)/\sqrt{6}$ where $\kappa = -7/144 - \mathrm{i}\sqrt{2}/36$, and $\operatorname{Re}\kappa \in [\frac{-7}{144}, \frac{1}{18}]$;*
- *hypercube diagonal $T = (1,1,1,1)/2$: $\operatorname{Im}\kappa = \frac{1}{12}\sum_\mu n_\mu^3$, nonzero for generic $\hat{n}$, with $|\operatorname{Im}\kappa| \le 1/(12\sqrt{3}) = 0.0481$, and $\operatorname{Re}\kappa \in [-1/24, -1/36]$.*

A complex κ means that a real wave number gives a complex frequency: the continued relation makes a plane wave grow or decay in that time parameter. A negative κ puts the phase velocity above the infrared limiting speed. Within these four classes, only axis time gives a real branch below the infrared speed in every spatial direction; it is the time used from here on.

Proof Recall (28). Assuming ω, k to both be parameters of the same order ϵ and expanding gives $\mathcal{L}(u) = (\mathrm{k}^2 - \omega^2) - \frac{1}{12}\sum_\mu(\mathrm{i}\omega T_\mu + \mathrm{k}n_\mu)^4 + O(\epsilon^6)$. Setting this to 0 and solving for ω with the positive root gives

$$\omega = \sqrt{\mathrm{k}^2 - \frac{1}{12}\sum_\mu(\mathrm{i}\omega T_\mu + \mathrm{k}n_\mu)^4 + O(\epsilon^6)}. \tag{69}$$

Using the lowest order solution $\omega = \mathrm{k}$ and expanding again gives

$$\omega = \mathrm{k}(1 - \frac{\sum_\mu u_\mu^4}{24}\mathrm{k}^2 + O(\epsilon^3)) \tag{70}$$

from which we can read off κ. Binomial expansion of $(n_\mu + \mathrm{i}T_\mu)^4$ gives (68). We have already covered the axis case $T = e_4$, $n_4 = 0$. The imaginary part vanishes, and $24\kappa = 1 + A$ with $A \in [\frac{1}{3}, 1]$. For the face diagonal: $\hat{n} \perp T$ forces $n_2 = -n_1$; write $n_1 = c_1/Z$, $n_2 = -c_1/Z$, $n_3 = c_2/Z$, $n_4 = c_3/Z$, where c_1, c_2, c_3 are real (only the time direction is imaginary) and $Z = \sqrt{2c_1^2 + c_2^2 + c_3^2}$ ensures normalization. Then

$$\kappa = \frac{-16c_1^4 - 8c_1^2\left(c_2^2 + c_3^2\right) + 3c_2^4 + 2c_2^2c_3^2 + 3c_3^4}{48\left(2c_1^2 + c_2^2 + c_3^2\right)^2}. \tag{71}$$

Simultaneously solving $\frac{\partial\kappa}{\partial c_1} = \frac{\partial\kappa}{\partial c_2} = \frac{\partial\kappa}{\partial c_3} = 0$ and only keeping real solutions c_1, c_2, c_3 gives a solution set $\{\{c_1 = c_2 = 0\}, \{c_1 = c_3 = 0\}, \{c_2 = c_3 = 0\}, \{c_1 = 0, c_3 = -c_2\}, \{c_1 = 0, c_3 = c_2\}\}$, for which $\kappa = \{\frac{1}{16}, \frac{1}{16}, \frac{-1}{12}, \frac{1}{24}, \frac{1}{24}\}$ respectively. The negative κ value corresponds to phase velocities above the infrared limit. The expression $\cosh(\omega/\sqrt{2}) = 1/\cos(\mathrm{k}/\sqrt{2})$ comes from evaluating (28) with the relevant face diagonal T and using $c_2 = c_3 = 0$ in the face diagonal $\hat{n}$.

If time is the body diagonal: orthogonality of T and $\hat{n}$ requires $n_1+n_2+n_3 = 0$, so one convenient parameterization is $\hat{n} = \frac{1}{Z}(c_1, c_2, -c_1 - c_2, c_3)$ where now $Z = \sqrt{2c_1^2 + 2c_1c_2 + 2c_2^2 + c_3^2}$ and

$$24\kappa = \frac{1}{3} + \frac{c_1^4 + (c_1 + c_2)^4 + c_2^4 + c_3^4}{Z^4} - \frac{4\left(c_1^2 + c_1c_2 + c_2^2\right)}{Z^2} - \frac{4\mathrm{i}\sqrt{3}c_1c_2(c_1 + c_2)}{Z^3}. \tag{72}$$

Setting the c_1, c_2, c_3 derivatives of the real and imaginary parts of κ to zero separately, making sure to only take roots where c_1, c_2, c_3 are all real, gives candidate solution sets from which the bounds may be computed

1. $\frac{-7}{144} \le \mathrm{Re}(\kappa) \le \frac{1}{18}$, where the extreme values are at the sets $\{c_3 = 0\}$ and $\{c_1 = c_2 = 0\}$ respectively.
2. $\frac{-\sqrt{2}}{36} \le \mathrm{Im}(\kappa) \le \frac{\sqrt{2}}{36}$, which take place at $\{c_2 = -2c_1, c_3 = 0\}$, $\{c_1 = -2c_2, c_3 = 0\}$ and $\{c_1 = c_2, c_3 = 0\}$. There is another zero gradient set $\mathrm{Im}(\kappa) = 0$ when $\{c_1 = c_2 = 0\}$.

Finally, on the hypercube diagonal: $\sum_\mu n_\mu = 0$ is required by orthogonality, so our parameterization can be $\hat{n} = (c_1, c_2, c_3, -c_1 - c_2 - c_3)/Z$ with $Z = \sqrt{c_1^2 + c_2^2 + c_3^2 + (c_1 + c_2 + c_3)^2}$. Now

$$\begin{aligned} 24\kappa =& \frac{1}{4} + \frac{c_1^4 + c_2^4 + c_3^4 + (-c_1 - c_2 - c_3)^4}{Z^4} - \frac{3(c_1^2 + c_2^2 + c_3^2 + (-c_1 - c_2 - c_3)^2)}{2Z^2} \\ & - 6\mathrm{i}\frac{(c_1 + c_2)(c_2 + c_3)(c_3 + c_1)}{Z^3} \end{aligned} \tag{73}$$

and performing the gradient calculations gives candidate solution sets and bounds as follows

1. $\frac{-1}{12\sqrt{3}} \le \mathrm{Im}(\kappa) \le \frac{1}{12\sqrt{3}}$, the bounding values occur at various permutations c_1, c_2, c_3 onto $-3d, d, d$ with $d \neq 0$
2. $\frac{-1}{24} \le \mathrm{Re}(\kappa) \le \frac{-1}{36}$. Here the maximum value occurs at $c_1 = c_2 = c_3$ and the c_1, c_2, c_3 onto $-3d, d, d$ with $d \neq 0$ permutations. The minimum value occurs at permutations of c_1, c_2, c_3 onto $-d, d, d$ for $d \neq 0$.

□

Figure 6 draws the four cases in the complex κ plane: the image of the sphere of propagation directions under (68) for each time direction. The axis image is a segment of the positive real line; the face-diagonal image is a real segment that crosses zero; the body- and hypercube-diagonal images are two-dimensional regions off the real line. The four ranges were also sampled at 2000 random directions per time axis (Appendix B); the samples fall inside the proved ranges and approach their endpoints.

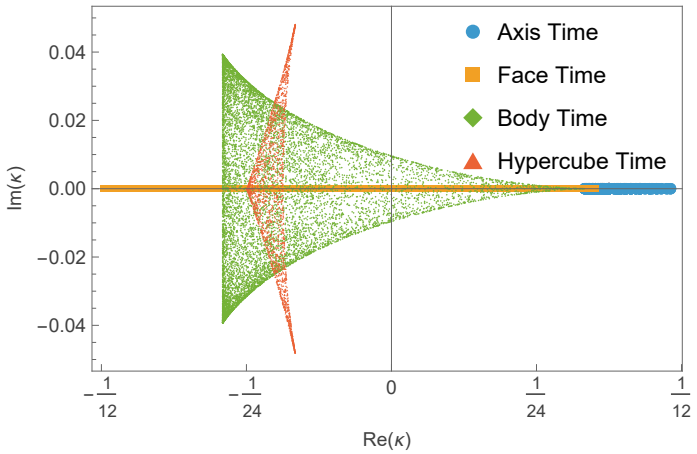

Fig. 6 The lowest order anisotropy coefficient κ of Theorem 5.4 for the four lattice directions as time. Each colored set is the image of the sphere of propagation directions $\hat{n} \perp T$ under (68). Axis time gives a real, positive segment: a real frequency and a subluminal phase velocity in every direction. Face-diagonal time gives a real segment crossing zero: superluminal in some directions. The two real segments are plotted at $\operatorname{Im}\kappa = 0$; the axis and face-diagonal segments have some overlap. Body- and hypercube-diagonal time give complex κ for almost every direction; the plot of these is generated by random sampling over the allowed $\hat{n}$ vectors.

5.4 Finite-momentum checks

Given a particular $(T, \hat{n})$, a numerical program solves for the eigenvalue of smallest modulus of the two-polarization Schur complement of the original edge symbol at $u = \mathrm{i}\omega T + \mathrm{k}\hat{n}$, defined in equation (131). The roots agree with $\mathcal{L}(u) = 0$ in the examples below. These checks test the implementation at finite momentum; the rank theorem itself follows from the exact algebra in Section 4.

5.5 What the branch says

With axis time, the analytically continued Euclidean symbol has two non-gauge null modes at every nonzero point on its characteristic branch. Both approach continuum TT gravitons and obey the same nonnegative real-frequency relation. The phase and group speeds stay below the infrared speed throughout the spatial zone. Other complex-frequency solutions related by the periodicity of the Euclidean symbol are not additional real-frequency branches.

Frame $(T;\hat{n})$	k	ω from $\mathcal{L}(u)=0$	$\lvert\omega_{\text{exact}}-\omega_{\mathcal{L}}\rvert$	5th, 6th— 7th
axis; $(1,2,3,0)/\sqrt{14}$	0.3	0.2983303963729907	1.0×10^{-46}	4e-41, 6e-41 | 0.044
	1.0	0.9439165855642197	2.2×10^{-47}	4e-41, 7e-41 | 0.438
	1.8	1.5286989076540076	2.2×10^{-47}	5e-41, 9e-41 | 1.09
	2.5	1.8954458498486524	1.0×10^{-47}	1e-40, 2e-40 | 1.43
face; $(1,-1,2,0)/\sqrt{6}$	1.0	1.0012383393165339	3.8×10^{-48}	3e-41, 7e-41 | 0.485
	2.5	2.6361751526267780	1.6×10^{-47}	1e-40, 1e-40 | 3.28
body; $(1,1,-2,0)/\sqrt{6}$	1.0	$1.05116987+0.04483252\,\mathrm{i}$	4.8×10^{-48}	5e-41, 5e-41 | 0.519
	2.5	$3.04156433+1.63054069\,\mathrm{i}$	$<10^{-47}$	2e-40, 4e-40 | 1.93

Table 4 Roots of the reduced symbol in the edge variables against roots of $\mathcal{L}(u)=0$, $u=\mathrm{i}\omega T+\mathrm{k}\hat{n}$, forty-digit arithmetic. Face time means $T=(1,1,0,0)/\sqrt{2}$; body time $T=(1,1,1,0)/\sqrt{3}$. The singular values of $\mathsf{E}(u)$ at the root in increasing order are: 1st to 4th the gauge zeros (all below 10^{-40}), 5th, 6th the two polarizations, 7th the first nonzero value.

For axis time the Euclidean lattice fixes this time law itself: by Proposition 5.2 and its following paragraph, the frequency (47) is the decay rate of Euclidean-time correlations of the two polarizations. A different time law needs a different lattice action. Considering instead a central second difference in real time (a discretization of $\partial_t^2\phi=\nabla^2\phi$) gives

$$\frac{4}{a_t^2}\sin^2(\omega a_t/2)=\frac{4}{a^2}\sum_j\sin^2(ak_j/2), \tag{74}$$

or $\omega=\frac{2}{a_t}\arcsin(\sqrt{\frac{a_t^2}{a^2}\sum_j\sin^2(ak_j/2)})$. Writing $r=a_t/a$, the small-momentum expansion of ω is $\omega=\mathrm{k}[1+(r^2-A)(\mathrm{k}a)^2/24+O((\mathrm{k}a)^4)]$.

A real frequency exists throughout the spatial zone only if $r\le1/\sqrt{3}$. At $r=1$, a real frequency exists only where $\sum_j\sin^2(ak_j/2)\le1$; the leading correction vanishes on axes and has the opposite sign on diagonals. The hyperbolic-sine relation in Theorem 5.1 and this temporal-sine recurrence are different time dynamics; only the first is produced by the Euclidean Kuhn action.

6 Direct Lorentzian propagation on the same triangulation

The choice of background geometry enters before the Fourier transform. Keeping the Kuhn simplices but replacing their Euclidean metric changes both the area derivatives and the dihedral-angle derivatives in the Regge Hessian. We now construct that Hessian on a flat Lorentzian background and compare its propagating modes with the continued Euclidean modes. Lorentzian Regge geometry and its integration contours also enter the one-loop path integral [20]; here we need only the second variation of the classical action.

6.1 Geometry, time and momentum

Write J_4 for the matrix with every entry equal to one and choose

$$g_L = I_4 - J_4, \qquad g_L^{-1} = I_4 - \tfrac{1}{3}J_4. \tag{75}$$

For an edge $D \in \{0,1\}^4 \setminus \{0\}$ with $n = \sum_\mu D_\mu$, its squared interval is $a^2 n(1-n)$. Table 5 lists the squared intervals, triangle areas, tetrahedron measures, four-simplex measure, and interior dihedral angles of one chain simplex at $a = 1$, and the same quantities for the Euclidean simplex on the same vertices. The four axis edges are null. The triangles, tetrahedra and four-simplices are nondegenerate; every triangle is timelike, so its normal plane is spacelike and the interior dihedral angle is an ordinary rotation angle. The end triangles 012 and 234 have angle $\pi/6$, and the middle triangle 123 has angle $2\pi/3$, in place of the Euclidean values $\pi/4$ and $\pi/2$. The angles around each hinge still sum to 2π. Null edges alone therefore do not prevent this second variation. On this branch the hinge areas are one half of the positive square root of minus the triangle Gram determinant, as in the Lorentzian column of the table, and the angle derivatives use that continuous flat branch.

The background (75), the Kuhn connectivity and variation of its squared edge lengths specify the model in this section. They are supplied geometric inputs to the propagation calculation. An overall factor $\sqrt{3}$ in the Hessian is immaterial to its kernel; let M_L be $\sqrt{3}$ times the midpoint symbol . Appendix A gives its rational cell matrix and assembly rule, so the following comparison does not require a continuation of M.

Use the unit timelike vector and unit spatial direction

$$\tau = \frac{(1,1,1,1)}{2\sqrt{3}}, \qquad \upsilon = \frac{(1,1,-1,-1)}{2}. \tag{76}$$

They satisfy $g_L(\tau,\tau) = -1$, $g_L(\upsilon,\upsilon) = 1$ and $g_L(\tau,\upsilon) = 0$. The direction $(1,1,1,1)$ is the only one fixed by every permutation of the axes, and it is timelike, $g_L((1,1,1,1),(1,1,1,1)) = -12$; τ is its unit vector. The components of υ sum to zero, so the J_4 term does not contribute to its norm.

We consider a wave vector

$$q^\mu = -\varpi\tau^\mu + K\upsilon^\mu \tag{77}$$

such that $\tau^\mu q_\mu = \varpi$ and $\upsilon^\mu q_\mu = K$. The associated covector to q^μ, written as a row vector in these coordinates, is

$$q = (z+t, z+t, z-t, z-t), \qquad t = K/2, \qquad z = \frac{\sqrt{3}\varpi}{2}, \tag{78}$$

the continuum null cone $q^\mu q_\mu = 0$ is $z = \sqrt{3}t$ and the phase speed $\varpi/K = z/(\sqrt{3}t)$. This fixes the physical clock and spatial normalization before comparing coefficients. Notice that the momentum covector in (78) has its first and second components equal

Table 5 Unit-spacing chain simplex, with vertices $v_0 = 0$ and $v_i = e_1 + \cdots + e_i$. The Euclidean metric is $\delta_{\mu\nu}$ and the Lorentzian metric is g_L. Edge entries are squared intervals. A d-dimensional measure is $\sqrt{|\det G_d|}/d!$, where G_d is the Gram matrix of d edges from one vertex of that face; for a triangle this is $\frac{1}{2}\sqrt{|\det G_2|}$, and the Lorentzian areas are the positive branch $\frac{1}{2}\sqrt{-\det G_h}$. The angle is the interior dihedral angle at that triangle, $\cos\theta_{ij} = -(G^{-1})_{ij}/\sqrt{(G^{-1})_{ii}(G^{-1})_{jj}}$ (the dihedral angles at triangles not containing vertex 0 need to be computed using a Gram matrix with a different base vertex). Restoring the spacing a multiplies a d-dimensional measure by a^d and does not change the angles.

	Euclidean		Lorentzian	
	measure	angle	measure	angle
Edges				
$01, 12, 23, 34$	1		0	
$02, 13, 24$	2		-2	
$03, 14$	3		-6	
04	4		-12	
Triangles				
012	$\frac{1}{2}$	$\pi/4$	$\frac{1}{2}$	$\pi/6$
013	$\frac{\sqrt{2}}{2}$	$\pi/2$	1	$\pi/2$
014	$\frac{\sqrt{3}}{2}$	$\pi/3$	$\frac{3}{2}$	$\pi/3$
023	$\frac{\sqrt{2}}{2}$	$\pi/2$	1	$\pi/2$
024	1	$\pi/2$	$\sqrt{3}$	$\pi/2$
034	$\frac{\sqrt{3}}{2}$	$\pi/3$	$\frac{3}{2}$	$\pi/3$
123	$\frac{1}{2}$	$\pi/2$	$\frac{1}{2}$	$2\pi/3$
124	$\frac{\sqrt{2}}{2}$	$\pi/2$	1	$\pi/2$
134	$\frac{\sqrt{2}}{2}$	$\pi/2$	1	$\pi/2$
234	$\frac{1}{2}$	$\pi/4$	$\frac{1}{2}$	$\pi/6$
Tetrahedra				
$0123,\ 1234$	$\frac{1}{6}$		$\frac{\sqrt{2}}{6}$	
$0124,\ 0134,\ 0234$	$\frac{\sqrt{2}}{6}$		$\frac{\sqrt{6}}{6}$	
Four-simplex				
01234	$\frac{1}{24}$		$\frac{\sqrt{3}}{24}$	

and its third and fourth components equal, we abbreviate these arguments

$$x = z + t, \quad y = z - t. \tag{79}$$

6.2 An exact cross-polarization branch

Let $b_1 = (1, -1, 0, 0)$ and $b_2 = (0, 0, 1, -1)$. Both are g_L-orthogonal to τ and υ, and they span the transverse plane of this wave. The edge strain of the cross polarization $h = b_1 \otimes b_2 + b_2 \otimes b_1$ is $c_D = D^{\mathsf{T}} h D$, that is

$$c_D = 2(D_1 - D_2)(D_3 - D_4), \tag{80}$$

where D_N are the components of the edge vector in class D. It is nonzero only on the four face diagonals $(0, 1, 0, 1), (0, 1, 1, 0), (1, 0, 0, 1), (1, 0, 1, 0)$, where its values are $+2, -2, -2, +2$. It is odd under each of the swaps $1 \leftrightarrow 2$ and $3 \leftrightarrow 4$.

Proposition 6.1 (Exact Lorentzian cross branch)**.** *For every real x, y,*

$$\mathsf{M}_L(x, x, y, y)c = s_\times(x, y)c, \qquad s_\times = -2 + \tfrac{3}{2}\cos x + \tfrac{3}{2}\cos y - \cos(x + y). \tag{81}$$

On (78), its characteristic equation is

$$2\cos^2 z - 3\cos z \cos t + 1 = 0. \tag{82}$$

For sufficiently small positive K, the branch approaching the continuum null cone is a nongauge zero mode and satisfies

$$v_\times(K) = 1 + \frac{5}{24}K^2 + o(K^2). \tag{83}$$

Proof On a paired covector the two swaps are lattice symmetries that fix q, so they commute with M_L. Their common odd subspace is one-dimensional, spanned by (80), so this vector is an eigenvector of $\mathsf{M}_L(x, x, y, y)$ at every x, y. Contracting the cell sum (124) with this column gives coefficients $-2, 3/2, 3/2, -1$ at frequencies $0, x, y, x + y$, respectively, and zero at all other frequencies. This gives (81); substituting $x = z + t$, $y = z - t$ gives (82).

Put $U = \sin^2(t/2)$ and $V = \sin^2(z/2)$, so that $\cos t = 1 - 2U$ and $\cos z = 1 - 2V$; zero momentum is $U = V = 0$. The characteristic equation (82) implies

$$G_\times(U, V) = 4V^2 - V + 3U - 6UV = 0. \tag{84}$$

Its derivative with respect to V at the origin is -1, so the implicit-function theorem selects a unique branch through the origin. Next, rewrite (84) in terms of K, ϖ, use the ansatz $\varpi = K + m_2 K^2 + m_3 K^3 + o(K^3)$, and take a series with respect to K. Canceling order by order gives $m_2 = 0$ and $m_3 = 5/24$, the phase velocity (83) follows from ϖ/K. Finally, in midpoint coordinates a vertex displacement has axis-edge components[3] $4\mathrm{i}\sin(q_\mu/2)\xi_\mu$, where ξ is the covector obtained from the displacement using g_L. All four sine factors are nonzero on this small positive branch. A gauge vector whose axis components vanish must therefore vanish entirely, whereas $c \neq 0$. The mode is nongauge. □

[3] See equation (9); with D is along an a lattice axis $D \cdot \xi$ selects the component of ξ along that axis

6.3 The second polarization and the comparison

The even sector under both swaps contains the plus polarization $b_1 \otimes b_1 - b_2 \otimes b_2$, and on the lattice it mixes there with the other even edge strains. Set the four axis-edge strains to zero as a gauge choice. This is possible whenever $\sin(x/2)$ and $\sin(y/2)$ are nonzero, because a vertex displacement shifts the axis strains by $4\mathrm{i}\sin(q_\mu/2)\xi_\mu$. The remaining swap-invariant vectors are constant on six edge orbits; the resulting matrix $B(x, y)$, the quadratic action restricted to these vectors, and its determinant are printed in Appendix A. In the same sine variables, its physical factor is

$$\begin{aligned} G_+(U,V) = {} & U^3(128V^3 - 192V^2 + 80V - 8) \\ & + U^2(-512V^4 + 832V^3 - 432V^2 + 88V + 20) \\ & + U(-512V^5 + 1792V^4 - 1584V^3 + 280V^2 + 20V - 6) \\ & + 1024V^6 - 2816V^5 + 2400V^4 - 648V^3 + 44V^2 + 2V. \end{aligned} \tag{85}$$

Since $\partial_V G_+(0,0) = 2$, it too has a unique branch through the origin. The gauge choice removes the four axis variables but not their four equations, so a root of $\det B$ must still be shown to give a mode of the full symbol. A nonzero vector in the kernel of B lifts to a nonzero vector in the kernel of M_L: swap symmetry gives the non-axis rows, and the lattice Bianchi identity gives the four axis rows. The same nonzero sine factors used above exclude a residual gauge vector. Expanding (85) at the origin in the clock (78) gives

$$v_+(K) = 1 - \frac{59}{24}K^2 + o(K^2), \qquad v_\times(K) - v_+(K) = \frac{8}{3}K^2 + o(K^2). \tag{86}$$

These are two actual small-momentum branches of the direct Lorentzian symbol along this ray. The cross mode is faster and the plus mode slower than the shared infrared speed. The calculation establishes birefringence in this direction; it does not classify the Lorentzian characteristic set at arbitrary momentum or direction.

The Euclidean calculation has a different result. On the axis-time continuation both polarizations have $v_E = 1-(1+A)K^2/24+O(K^4)$ and remain degenerate. Even if one instead continues along the Euclidean hypercube diagonal $T = (1,1,1,1)/2$ with the paired spatial direction v, (68) gives $v_E = 1+K^2/24+O(K^4)$ for both modes. Neither continuation gives (86). The metric, the clock and the Hessian must all be specified before a lattice graviton dispersion relation is interpreted as a physical prediction. The cosmic-ray calculation below consequently remains a conditional application of the axis-time Euclidean branch. Applying a radiation bound to (86) requires its own matter dispersion, vertex and polarization sum.

7 Matter sources must satisfy the gravitational constraints

The vacuum calculation determines the free gravitational branch. A sourced calculation also needs matter to respond to the same edge geometry. The following construction

shows that consistent matching is nontrivial. It is an explicit Euclidean scalar model; it does not provide the fermion emission vertex assumed in Section 8.

7.1 The scalar model

Use one shared assignment of squared edge lengths a_e on a finite periodic Kuhn lattice, with at least three cells in each direction (so no simplex connects with its periodic image). On a simplex with ordered vertices $v_0, \dots, v_4$, write $a_{ij} = a_{\{v_i, v_j\}}$ and $a_{ii} = 0$. Define

$$G_{ij} = \frac{a_{0i} + a_{0j} - a_{ij}}{2}, \qquad E^{ij} = (G^{-1})_{ij}, \qquad V_\sigma = \frac{\sqrt{\det G}}{24}, \quad i, j = 1, \dots, 4. \tag{87}$$

Here G is required to be positive definite. Its entries are the scalar products of the four edges from v_0; shared edge lengths therefore give matching intrinsic metrics on shared faces. On the unit flat Kuhn simplex, $a_{0i} = i$, $a_{ij} = |i - j|$, and hence

$$G_{ij} = \min(i, j), \qquad E = \begin{pmatrix} 2 & -1 & 0 & 0 \\ -1 & 2 & -1 & 0 \\ 0 & -1 & 2 & -1 \\ 0 & 0 & -1 & 1 \end{pmatrix}, \qquad V_\sigma = \frac{1}{24}. \tag{88}$$

All squared lengths in this example are positive Euclidean lengths.

Attach to each vertex v an unconstrained field $\phi_v \in \mathbb{C}^r$. To compare fields living at different vertices, prescribe a unitary $U_{ij} \in U(r)$ on each axis edge, carrying from vertex j to vertex i, with $U_{ij} = U_{ji}^{-1}$. These U links are external data and are held fixed in every variation below.

Within a simplex, we compare everything in the frame at the base vertex v_0. The Kuhn ordering $v_0, v_1, \dots, v_4$ makes every consecutive step an axis edge, so the transport from v_i back to v_0 is the ordered product along that path,

$$W_0 = I_r, \qquad W_i = W_{i-1} U_{v_{i-1} v_i} = U_{v_0 v_1} U_{v_1 v_2} \cdots U_{v_{i-1} v_i}, \tag{89}$$

the rightmost factor acting first. Write

$$w_i = W_i \phi_{v_i} - \phi_{v_0}, \qquad i = 0, \dots, 4, \tag{90}$$

for the displacement of the ith vertex field from the base field, both read at v_0. Notice that (90) gives $w_0 = 0$. Consecutive displacements differ by a single link,

$$w_i - w_{i-1} = W_{i-1}\big(U_{v_{i-1} v_i} \phi_{v_i} - \phi_{v_{i-1}}\big). \tag{91}$$

As a product of unitary Us, W_{i-1} is itself unitary, so the norms agree,

$$\|w_i - w_{i-1}\| = \big\|U_{v_{i-1} v_i} \phi_{v_i} - \phi_{v_{i-1}}\big\|. \tag{92}$$

The right-hand side is the covariant difference of the two vertex fields across the single axis edge (v_{i-1}, v_i), written in the frame at v_{i-1}. That equality of norms is the only property of W used in the flat reduction below.

Under a local change of frame $R_v \in U(r)$, with $\phi_v \mapsto R_v \phi_v$ and $U_{st} \mapsto R_s U_{st} R_t^\dagger$, each $W_i \mapsto R_{v_0} W_i R_{v_i}^\dagger$, hence every $w_i \mapsto R_{v_0} w_i$ and the action is unchanged.

For constants γ and $\kappa_m > 0$, take

$$S[a, \phi; U] = \gamma \sum_h A_h(a)\delta_h(a) + S_m[a, \phi; U], \qquad S_m = \frac{\kappa_m}{2} \sum_\sigma V_\sigma \sum_{i,j=1}^{4} E_\sigma^{ij} \operatorname{Re}\langle w_i, w_j \rangle. \tag{93}$$

This is a proposed coupled action, with its transport rule stated above. The same a_e determine the Regge geometry and the scalar weights V_σ. Positive definiteness of G makes the scalar quadratic form nonnegative. Setting every link to the identity removes the background gauge field: $W_i = I_r$ and $w_i = \phi_{v_i} - \phi_{v_0}$, so S_m reduces to the Dirichlet energy of a piecewise affine field $\phi : \mathbb{Z}^4 \to \mathbb{C}^r$.

Label $(B_\sigma)_{ij} = \operatorname{Re}\langle w_i, w_j \rangle$ as the real symmetric 4×4 Gram matrix of the transported displacements, then

$$\operatorname{tr}(E_\sigma B_\sigma) = \sum_{i,j=1}^{4} E_\sigma^{ij} \operatorname{Re}\langle w_i, w_j \rangle, \tag{94}$$

because E_σ and B_σ are both symmetric. Since $w_0 = 0$, we can use the explicit form of E from (88) to reduce (94), giving

$$\sum_{i,j} E^{ij} \operatorname{Re}\langle w_i, w_j \rangle = \sum_{i=1}^{4} \|w_i - w_{i-1}\|^2 = \sum_{i=1}^{4} \|U_{v_{i-1}v_i}\phi_{v_i} - \phi_{v_{i-1}}\|^2. \tag{95}$$

The last equality uses unitarity of each prefix transport. On the periodic unit lattice, summing cancels the volume factor $1/24$, thus

$$S_m = \frac{\kappa_m}{2} \sum_{\text{positive axis edges } (s,t)} \|U_{st}\phi_t - \phi_s\|^2. \tag{96}$$

For identity links this is $\frac{\kappa_m}{2} \sum_{x,\mu} |\phi(x + e_\mu) - \phi(x)|^2$, whose Fourier symbol is $\kappa_m \mathcal{L}(k)$. This connects the example to the gravitational characteristic factor. It also shows why the conventional-matter assumption in the Cherenkov bound is additional: applying the same time continuation to this scalar would give the same free scalar and graviton frequency relation.

For the edge variation at fixed fields and links,

$$\delta E = -E(\delta G)E, \qquad \delta V_\sigma = \tfrac{1}{2} V_\sigma \operatorname{tr}(E\delta G), \tag{97}$$

so

$$\delta_a S_m = \frac{\kappa_m}{2} \sum_\sigma V_\sigma \left[\frac{1}{2} \operatorname{tr}(E\delta G) \operatorname{tr}(EB) - \operatorname{tr}(E\delta G E B) \right]. \tag{98}$$

Every local squared edge has a specified variation $\delta G_{ij} = (\delta a_{0i} + \delta a_{0j} - \delta a_{ij})/2$. After assembly on shared edges, the Schläfli identity gives

$$\gamma \sum_{h \supset e} \delta_h \frac{\partial A_h}{\partial a_e} + \frac{\partial S_m}{\partial a_e} = 0. \tag{99}$$

The vertex fields must also be varied. On the unit flat lattice the scalar action has already reduced to (96), a sum of squared covariant differences over axis edges. Differentiating $\|U_{st}\phi_t - \phi_s\|^2$ with respect to $\langle \phi_x|$ produces $\phi_x - U_{xt}\phi_t$ from each axis neighbor t of x, so stationarity reads

$$\sum_{\mu = \pm e_1, \ldots, \pm e_4} \left(\phi_x - U_{x,x+\mu} \phi_{x+\mu} \right) = 0 \tag{100}$$

at every vertex x. For identity links this is $\mathcal{L}\phi = 0$. Because S_m is homogeneous of degree two in ϕ, contracting (100) with ϕ returns a multiple of S_m. Stationarity therefore forces $S_m = 0$. Each simplex contribution is $V_\sigma w^\dagger E_\sigma w$ with $E_\sigma \succ 0$, so every $w_i = 0$, hence $B_\sigma = 0$ and the edge source in (99) vanishes. Nonconstant stationary fields require, for example, prescribed boundary data on a lattice with boundary.

Equations (99) and (100) are the coupled stationary equations of the stated action.

7.2 The null-space compatibility condition

Proposition 7.1. *Let* H *be the symmetric flat gravitational Hessian. A solution of* $\gamma \mathsf{H} \delta a = -J$ *requires* $n^\mathsf{T} J = 0$ *for every* n *with* $\mathsf{H} n = 0$.

Proof Multiplying by n^T gives $-n^\mathsf{T} J = \gamma n^\mathsf{T} \mathsf{H} \delta a = \gamma (Hn)^\mathsf{T} \delta a = 0$. □

This is a condition on the source in the linearized equation. Solving the scalar field equation on the background alone need not satisfy it. The flat vertex-displacement symmetry used here should also be distinguished from the broken gauge symmetries and pseudo-constraints that can occur on curved Regge backgrounds [16].

7.3 Two harmonic sources that violate compatibility

Certain values of vertex fields and links cannot be consistently coupled to the gravitational sector in the linearized theory. We give two explicit examples here involving identity links. The two fields below are not periodic. Since a periodic lattice admits only constant stationary fields, these examples are posed on a lattice with boundary, with boundary vertex values given by the same formulas and the equations imposed at interior vertices and edges; the infinite lattice gives the same statements.

The first obstruction is on a single hypercube. Recall Theorem 3.1 that the $\frac{\partial A_h}{\partial a_e} = 0$ when $e = 1111$ is the hypercube diagonal. Any field satisfying equation (99) would

then need to obey $\frac{\partial S_m}{\partial a_{1111}} = 0$ for the lowest order perturbations about flat space, or equivalently the sum in (98) must vanish. However, consider the field

$$\phi(x) = \lambda(x_1 + x_2), \tag{101}$$

which is exactly harmonic $\mathcal{L}(\phi) = 0$, so (100) is satisfied. The matrix B_σ is, for instance,

$$B_\sigma = \begin{pmatrix} 1 & 2 & 2 & 2 \\ 2 & 4 & 4 & 4 \\ 2 & 4 & 4 & 4 \\ 2 & 4 & 4 & 4 \end{pmatrix} \lambda^2 \tag{102}$$

on the simplex with vertices $(0,0,0,0), (1,0,0,0), (1,1,0,0), (1,1,1,0), (1,1,1,1)$, the other twenty three simplices of the hypercube will have their own B_σ. The δG for variation of the hypercube diagonal is

$$\begin{pmatrix} 0 & 0 & 0 & \frac{1}{2} \\ 0 & 0 & 0 & \frac{1}{2} \\ 0 & 0 & 0 & \frac{1}{2} \\ \frac{1}{2} & \frac{1}{2} & \frac{1}{2} & 1 \end{pmatrix} \delta a_{1111} \tag{103}$$

Performing all the matrix and simplex sums in (98) and putting the answer into (99) gives

$$0 - \frac{\kappa_m \lambda^2}{12} = 0 \tag{104}$$

which requires $\lambda = 0$ (no field) or $\kappa_m = 0$ (no coupling). For $\kappa_m \lambda^2 \neq 0$, the linearized gravitational edge equation therefore has no solution for this fixed scalar profile and identity links. This conclusion concerns the flat Hessian equation; it does not exclude nonlinear backreaction or a coupled change of the matter configuration.

For the second obstruction, consider another harmonic vertex field

$$\phi = \lambda(x_1^3 - 3x_1 x_2^2) \tag{105}$$

and moving the vertex $p = (0,1,0,0)$ along $\xi = e_1 - e_3$ by ϵ for the deformation. Define vectors J and g with components $J_e = \frac{\partial S_m}{\partial a_e}$ and $g_D = \pm 2D \cdot \xi$, where the $+$ sign is if p is the head of the edge and $-$ if p is the tail. Because g is a gauge vector, the associated gravitational action at this order is zero, but the associated matter action is not because

$$g^{\mathsf{T}} J = -18\kappa_m \lambda^2. \tag{106}$$

Notice that we will have to sum over all 120 simplices containing p. Every hypercube diagonal incident to that vertex has $D \cdot \xi = 0$, so deleting the diagonal variable does not cancel the contraction. Once again the linearized edge equation has no solution.

Both obstructions are instances of one solvability condition. At first order about flat space, (99) reads $\gamma\,(\mathsf{H}\,\delta a)_e = -J_e$, with H the flat Hessian of Section 2, which is symmetric. A solution exists only if J is orthogonal to every null vector of H. The

hypercube-diagonal strain and the vertex displacements are such null vectors, and the two fields violate exactly these two conditions. The value of $g^{\mathsf{T}}J$ depends on the vertex; for the same field it vanishes at the origin.

8 A conditional gravitational Cherenkov bound

8.1 Standard-Model Extension coefficients

Let $p = |\mathbf{p}|$ be a physical wave number, $q = ap$ the dimensionless lattice wave number, and $\hat{p} = \mathbf{p}/p$. In this section $\hbar = c_{\mathrm{IR}} = 1$, so p and ω have units GeV and a has units GeV^{-1}; $1\,\mathrm{GeV}^{-1} = 1.97327 \times 10^{-16}$ m. The axis-time branch in physical units is

$$\omega(\mathbf{p}) = \frac{2}{a}\,\mathrm{arcsinh}\sqrt{\sum_j \sin^2(ap_j/2)}, \qquad \frac{\omega}{p} = 1 - \kappa(\hat{p})a^2p^2 + O(a^4p^4). \tag{107}$$

Kostelecký and Tasson (KT) write, to first order in the Lorentz-violating coefficients, a gravitational wave refraction index $n_g = 1 - \frac{1}{2}\sum_d (-1)^{d/2} s^{(d)}(\hat{p}) p^{d-4}$ [15], equations (20)–(21). For mass dimension $d = 6$ this gives

$$n_g(\hat{p}, p) = \frac{p}{\omega} = 1 + \tfrac{1}{2}p^2 s^{(6)}(\hat{p}) + O(a^4p^4), \qquad [s^{(6)}] = \mathrm{GeV}^{-2}. \tag{108}$$

Matching phase velocities with our earlier results yields

$$s^{(6)}(\hat{p}) = 2\kappa(\hat{p})a^2 = \frac{1 + A(\hat{p})}{12}a^2. \tag{109}$$

It can be convenient to break $s^{(6)}$ into spherical harmonics:

$$s^{(6)}(\hat{p}) = \sum_{jm} Y_{jm}(\hat{p}) s^{(6)}_{jm}. \tag{110}$$

Kostelecký and Mewes (KM) instead write the nonbirefringent branch as $\omega = p(1-\varsigma^0)$, with $\varsigma^0 = \omega^2 \sum_{jm} Y_{jm}(\hat{n}_{\mathrm{sky}}) k^{(6)}_{(I)jm}$ and $\hat{n}_{\mathrm{sky}} = -\hat{p}$ [21], equations (5) and (7). At this order ω^2 can be replaced by p^2. Since $Y_{jm}(-\hat{p}) = (-1)^j Y_{jm}(\hat{p})$, the conventions are related by

$$k^{(6)}_{(I)jm} = \tfrac{1}{2}(-1)^j s^{(6)}_{jm}. \tag{111}$$

Only $j = 0, 4$ occur below, so every listed KM coefficient is half the KT coefficient.

The function $A(\hat{n}) = \sum_j n_j^4$ has full cubic symmetry, so its spherical content is $j = 0$ and $j = 4$ only, with the $j = 4$ components fixed up to one number. With the standard complex spherical harmonics Y_{jm} (reality gives $s_{4,-4} = \overline{s_{44}}$; here azimuthal reflection also makes these coefficients real) in a frame aligned with the lattice axes,

$$s^{(6)}_{00} = \frac{4\sqrt{\pi}}{15}a^2 = 0.4727\,a^2, \qquad s^{(6)}_{40} = \frac{\sqrt{\pi}}{45}a^2 = 0.03939\,a^2, \qquad s^{(6)}_{4,\pm4} = \sqrt{\tfrac{5}{14}}\,s^{(6)}_{40} = 0.02354\,a^2, \tag{112}$$

unlisted components are zero in this frame. In a real basis the single $m = 4$ cosine harmonic $(Y_{44}+Y_{4,-4})/\sqrt{2}$ carries $\sqrt{5/7}\, s^{(6)}_{40} = 0.03329\, a^2$. The mean over directions of (109) is $(1 + \frac{3}{5})a^2/12 = 2a^2/15$. Because κ and $s^{(6)}$ are directly proportional, Figure 4 illustrates this pattern: six maxima on the lattice axes, eight minima on the body diagonals, twelve saddles on the face diagonals, the $j = 4$ cubic harmonic on top of its mean.

8.2 Gravitational Cherenkov radiation

A particle moving faster than the phase velocity of gravitational waves could hypothetically radiate gravitons and lose energy [22]. A subluminal graviton, $v_{\mathrm{ph}} < 1$, is therefore constrained by the arrival of the highest-energy cosmic rays: a parton of energy E_f that has traveled a distance L can only have arrived if its Cherenkov loss over L was small. Kostelecký and Tasson worked out the rate for a graviton with $s^{(d)}$ coefficients [15]; for $d = 6$ the condition that a parton of energy E_f survives a distance L in direction $\hat{p}$ is

$$s^{(6)}(\hat{p}) < \left(\frac{\mathcal{F}_\psi(6)}{G_{\mathrm{N}}\, E_f^7\, L}\right)^{1/2}, \qquad \mathcal{F}_\psi(d) = \frac{(d-2)(d-3)(2d-3)}{4(2d^2-7d+9)}, \quad \mathcal{F}_\psi(6) = \frac{9}{13}, \tag{113}$$

with $G_{\mathrm{N}} = 1/E_{\mathrm{P}}^2$, $E_{\mathrm{P}} = 1.2209 \times 10^{19}$ GeV [23]; the factor $\mathcal{F}_\psi$ is the fermion emission integral of [15], and $s^{(6)}(\hat{p})$ is the value (109) in the arrival direction. Note the results from (113) are imported; we examine the applicability conditions to our case in more detail in Subsection 8.5. The factor $\mathcal{F}_\psi$ brings with it the polarization sum, the standard fermion dispersion, and the minimal vertex of that calculation. The directional coefficient $s^{(6)}$ is the quantity computed from the continued symbol. Inverting (113) with (109), the spacings excluded by a parton of energy E_f from distance L are

$$a > a_{\mathrm{thr}}(E_f, L, \hat{p}) = \left(\frac{12}{1 + A(\hat{p})}\right)^{1/2} \left(\frac{\mathcal{F}_\psi(6)}{G_{\mathrm{N}}\, E_f^7\, L}\right)^{1/4} \propto E_f^{-7/4} L^{-1/4}. \tag{114}$$

The steep $E_f^{-7/4}$ is why the highest-energy events carry the bound.

8.3 The bound

We use the 3.2×10^{20} eV Fly's Eye event [24]; the Pierre Auger composition analysis indicates a trend toward heavier primaries in its high-energy sample, with hadronic-model dependence [25]. The energy that enters (113) is that of a single parton, a fraction r of the energy per nucleon, and the distance L is that of the source; neither is measured event by event. Kostelecký and Tasson's conservative reading takes the Fly's Eye event to be an iron nucleus whose leading parton carries a tenth of the per-nucleon energy ($E_f = E/560 = 5.7 \times 10^{17}$ eV) from a source at 10 Mpc [15]; in (113) that gives

$$s^{(6)}(\hat{p}) < 5.8 \times 10^{-32}\, \mathrm{GeV}^{-2} \tag{115}$$

in the arrival direction, and for the isotropic coefficient $s_{00}^{(6)} = \sqrt{4\pi}\, s^{(6)}(\hat{p}) < 2.0 \times 10^{-31}\,\mathrm{GeV}^{-2}$, the published bound. The lattice value (109) is at least $a^2/9$ in every direction (the body diagonal, $A = \frac{1}{3}$), so whatever the arrival direction,

$$a^2 < 9 \times 5.8 \times 10^{-32}\,\mathrm{GeV}^{-2},$$
$$a < 7.2 \times 10^{-16}\,\mathrm{GeV}^{-1} = 1.42 \times 10^{-31}\,\mathrm{m} = 8.8 \times 10^{3}\,\ell_{\mathrm{P}}, \qquad \frac{1}{a} > 1.39 \times 10^{15}\,\mathrm{GeV}. \tag{116}$$

Along an axis the same event gives $a < 1.16 \times 10^{-31}$ m. The value $a < 1.3 \times 10^{-31}$ m obtained by comparing only $s_{00}^{(6)}$ with an isotropic-only fit is a benchmark, since the lattice also has correlated $j = 4$ coefficients. Equation (116) uses the minimum of the full directional coefficient and holds without knowing the lattice orientation. Table 6 shows how the bound tightens under less conservative readings: a proton primary with $r = 0.1$ excludes spacings above $6.3\,\ell_{\mathrm{P}}$ (10 Mpc) or $3.5\,\ell_{\mathrm{P}}$ (100 Mpc); a 10^{20} eV parton excludes $a > 0.85\,\ell_{\mathrm{P}}$ or $a > 0.48\,\ell_{\mathrm{P}}$, both below the Planck length; a proton carrying its whole energy in one parton would exclude the Planck spacing by a factor 9 to 16. Figure 7 shows the exclusion plane.

Parton assumption for the 320 EeV event	E_f (eV)	$a_{\mathrm{thr}}/\ell_{\mathrm{P}}$, $L = 10$ Mpc	$a_{\mathrm{thr}}/\ell_{\mathrm{P}}$, $L = 100$ Mpc
iron, $r = 0.1$ (the reading of [15])	5.7×10^{17}	7.2×10^{3}	4.0×10^{3}
proton, $r = 0.1$	3.2×10^{19}	6.3	3.5
proton, $r = 0.31$ ($E_f = 10^{20}$ eV)	1.0×10^{20}	0.85	0.48
proton, $r = 1$	3.2×10^{20}	0.11	0.063

Table 6 Lattice spacings excluded ($a > a_{\mathrm{thr}}$) by the survival of the Fly's Eye event, from (114) along an axis ($A = 1$). Along a body diagonal a_{thr} is larger by $(2/(4/3))^{1/2} = 1.22$; the first row times 1.22 is the direction-independent bound (116).

It is worth comparing the bounds on lattice size implied by this graviton Cherenkov analysis with those obtained through other means in [6], which examines the possibility of a hypercubic grid and examines bounds on the lattice size based on several different measurements. They conclude, for instance, that the anomalous magnetic moment of the muon gives constraints of $1/a \geq 3.6 \times 10^{7}$GeV, the Rydberg constant gives constraints $1/a \geq 4 \times 10^{8}$GeV, and analysis of the GZK cutoff gives a constraint of $1/a \geq 10^{11}$GeV. While the gravitational Cherenkov bounds computed above are more stringent, it needs to be kept in mind that their bounds are contingent on their own particular processes and assumptions, not ours.

8.4 What a Planck-scale spacing predicts

At $a = \ell_{\mathrm{P}}$, $s^{(6)}(\hat{n})$ lies between 7.5×10^{-40} and $1.1 \times 10^{-39}\,\mathrm{GeV}^{-2}$, a factor 5×10^{7} inside (115). The loss over the assumed travel distance becomes constraining for partons above

$$E_f > 9.1 \times 10^{19}\ \mathrm{eV} \quad (\text{axis},\ L = 10\ \mathrm{Mpc}),$$

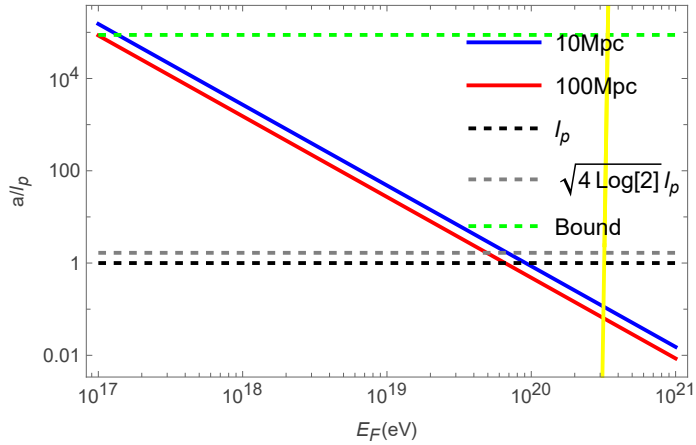

Fig. 7 The exclusion plane. A parton of energy E_f that has crossed L excludes all spacings above the line, equation (114). The vertical line is the Fly's Eye event energy; the parton energy is that times the fraction r per nucleon. The uppermost dashed "Bound" line corresponds to (116), the Planck length ℓ_{P} and spacing $\sqrt{4\log(2)}\ell_{\mathrm{P}}$ are the lower dashed lines. A Planck-scale spacing is excluded once a parton above 9.1×10^{19} eV (10 Mpc) or 6.6×10^{19} eV (100 Mpc) in an axis direction is established.

$$E_f > 1.02 \times 10^{20}\ \text{eV} \quad (\text{body diagonal},\ L = 10\ \text{Mpc}),$$
$$E_f > 6.6 \times 10^{19}\ \text{eV} \quad (\text{axis},\ L = 100\ \text{Mpc}).$$

A proton of 10^{20} eV has $1 - v = 4.4 \times 10^{-23}$, and outruns the Planck-lattice graviton only for graviton wave numbers above 2.8×10^8 GeV for an axis direction; the emitted gravitons are hard, which is what makes the loss rate steep in E_f. They are still long compared with the lattice: the hardest graviton has $p \le E_f \approx 10^{11}$ GeV, so $pa \le 10^{-8}$ at a Planck spacing, and the term (48) gives the leading dispersion defect, whose higher-order relative correction is of order 10^{-16} throughout the Cherenkov integral. The bound is one-sided: survival above the relevant loss scale constrains this subluminal branch under the stated matter and source assumptions. Gravitational-wave detectors do not constrain a at this level: at $p = 2\pi \times 100\,\mathrm{Hz}/c = 2 \times 10^{-6}\,\mathrm{m}^{-1}$ the defect $\kappa p^2 a^2$ is 10^{-82} at a Planck spacing.

8.5 What the bound rests on

The Cherenkov argument compares the parton's velocity with the graviton's phase velocity. It assumes conventional ultrarelativistic matter dispersion[4], with no additional Lorentz-violating term large enough to change the emission kinematics [15, 22]; a dispersive matter sector changes this comparison and the emission phase space. For massless collinear kinematics with $E_m(p) = p - \alpha_m p^3$ and $\omega_g(\rho) = \rho - \alpha_g \rho^3$, the available energy is $-3\alpha_m p\rho(p - \rho) + (\alpha_g - \alpha_m)\rho^3$. Equal positive cubic coefficients close this channel at this order; changing a sign changes the kinematics and rate, rather than simply doubling a bound.

[4]An alternate approach with matter fields defined on the lattice would generally result in modified dispersion. The bound in this section is for conventional fermions.

9 A candidate lattice spacing

One idea for the spacing of the Kuhn lattice that returns a spacing close to, but not exactly, the Planck scale comes from black hole thermodynamics. The standard form of the Bekenstein Hawking entropy [26, 27] is

$$S = \frac{k_b c^3 A}{4G\hbar} = k_b \frac{A}{4\ell_p^2}. \tag{117}$$

Consider a system with N bits, the Boltzmann entropy will be $S = k_b \ln(2^N)$. Equating the Boltzmann and Bekenstein-Hawking entropy gives

$$N = \frac{A}{4\ln(2)\ell_p^2}. \tag{118}$$

Supposing the lattice spacing has one bit per axis edge square face [5], a horizon patch of area A aligned with a coordinate plane carries $N = A/a^2$ bits, and equating the two counts gives

$$a = \sqrt{4\ln(2)}\ell_p \approx 1.665\ell_p. \tag{119}$$

The count is per face, not per unit hinge area. The triangles of the Kuhn triangulation are right triangles with legs $\sqrt{r}$ and $\sqrt{q}$, $(r, q) = (1, 1), (1, 2), (1, 3), (2, 2)$, so their areas are $\frac{1}{2}$, $\frac{\sqrt{2}}{2}$, $\frac{\sqrt{3}}{2}$ and 1, and the first two have no common area quantum. The lattice staircase that approximates a plane patch with unit normal $\hat{\nu}$ in a spatial slice has $\sum_j |\nu_j| \geq 1$ axis faces per unit area, with equality only when the patch is aligned, so the value above is the aligned normalization. This basic line of reasoning has been considered before (see for instance [29–31]). We will refer to this as "bit spacing" as a shorthand.

The measured value of G supplies the SI anchor $a = 2.6912 \times 10^{-35}$ m and $E_{\rm lat} = \hbar c/a = E_{\rm P}/\sqrt{4\ln 2} = 7.3322 \times 10^{18}$ GeV; the relation fixes $a/\ell_{\rm P}$. The face-record count fixes the normalization; the remaining premise is the identification of the Regge edge with the bit-spacing edge.

At this spacing, $s^{(6)}(\hat{n})$ ranges from 2.067×10^{-39} to 3.100×10^{-39} GeV^{-2}, at least a factor 1.86×10^7 below the conservative directional limit. The attenuation energies are 6.82×10^{19} eV (axis, 10 Mpc), 7.66×10^{19} eV (body diagonal, 10 Mpc), and 4.91×10^{19} eV (axis, 100 Mpc). Under the matter and coupling premises of Section 8, a parton above 7.66×10^{19} eV known to have traveled at least 10 Mpc (for instance, the bottom two rows of Table 6, reading the Fly's eye event as a proton) would therefore exclude this spacing for every lattice orientation. These are propagation-loss scales, not sharp kinematic emission thresholds; their distance dependence comes from accumulated energy loss.

[5] One bit per axis square face is the count of an explicit record structure. Put a binary variable on each vertex of an $m \times n$ patch of axis squares and let each face record the parity of its four corners. Over the two-element field this map from corner values to face records has rank mn: with the corners of the first row and column fixed, each further corner completes one face and can be chosen to give that face either parity. The face records therefore carry exactly one independent bit per face [28]

9.1 Photon and graviton propagation

A continuous-time spatial-lattice wave model was considered in [32], which we will reference as model $\gamma 1$. It has $\omega_{\gamma 1}(\mathrm{k}) = \mathrm{k} - A(\hat{n})a^2\mathrm{k}^3/24 + O(a^4\mathrm{k}^5)$. Model $\gamma 1$ uses the same spacing, $a = \sqrt{4\ln 2}\,\ell_p$, and comparing it with the continued graviton branch, it gives

$$v_{\mathrm{ph},\gamma 1}(\mathrm{k}) - v_{\mathrm{ph},g}(\mathrm{k}) = \frac{a^2\mathrm{k}^2}{24} + O(a^4\mathrm{k}^4). \tag{120}$$

This compares equal wave numbers under two stated time laws. Conversely, [33] examines another lattice wave model (which we will refer to as $\gamma 2$) and the associated deviations from continuum electromagnetic waves. Model $\gamma 2$ uses the same spacing again, and its frequency is $\omega_{\gamma 2}(\mathrm{k}) = (2/a)\,\mathrm{arcsinh}\sqrt{\sum_j \sin^2(k_j a/2)}$, which is (47) exactly; in both cases it is the Euclidean lattice transfer energy of a nearest-neighbor field (Proposition 5.2 and its following paragraph). Therefore, the complexified Kuhn gravitons considered in this paper would have identical phase and group velocities at every wave number to photons within the $\gamma 2$ model.

The differing laws also allow a definite kinematic test of photon emission. Let an incoming photon of momentum $p\hat{n}$ emit a collinear graviton of momentum $yp\hat{n}$, with $0 < y < 1$, leaving a photon of momentum $(1-y)p\hat{n}$. At leading order in ap the excess energy is

$$\omega_{\gamma 1}(p) - \omega_{\gamma 1}((1-y)p) - \omega_g(yp) = \frac{a^2p^3}{24}\,y\big(y^2 + 3Ay - 3A\big) + O(a^4p^5). \tag{121}$$

It is positive for $y > y_* = (\sqrt{9A^2+12A}-3A)/2$, where $y_* \in [(\sqrt{5}-1)/2, (\sqrt{21}-3)/2] \simeq [0.6180, 0.7913]$ for $1/3 \le A \le 1$. A small noncollinear angle then reduces the available energy, allowing energy and momentum conservation for a hard emitted graviton when $ap \ll 1$ and y lies above this boundary. Conversely,

$$\omega_{\gamma 2}(p) - \omega_{\gamma 2}((1-y)p) - \omega_g(yp) = \frac{a^2p^3}{8}(1+A)y(y-1) + O(a^4p^5). \tag{122}$$

For fixed $0 < y < 1$ the leading coefficient is negative. Thus, at sufficiently small ap, this collinear channel has no kinematic opening at the stated order. There is a kinematic opening in the case of model $\gamma 1$, but we have not computed an emission rate. Kostelecký and Tasson give scalar, fermion and photon rates [15], with conventional matter dispersion; using the modified photon law here requires its vertex and phase-space calculation. The fermion attenuation bound cannot be transferred to photons merely by comparing equal-momentum phase velocities.

10 Discussion and conclusion

The same simplicial connectivity supports different graviton propagation laws when its background geometry is changed. On the Euclidean Kuhn lattice the exact characteristic factor is the scalar lattice Laplacian. The rank proof counts two nongauge modes on its nonzero complex cone. With axis time they have equal frequencies and phase and

group speeds bounded by the infrared speed throughout the spatial Brillouin zone. Their decay-rate interpretation belongs to the positive free TT Gaussian with the stated sign choice.

On the direct Lorentzian background $g_L = I_4 - J_4$, the paired ray has two distinct small-momentum branches. Their phase coefficients are $5/24$ and $-59/24$ in the unit timelike frame. The cell matrix, assembly rule and reduced determinant make this distinction explicit. An analytic continuation of the Euclidean characteristic equation therefore does not supply this Lorentzian result. A classification in general spatial directions remains a separate calculation; the paired ray alone establishes the polarization splitting claimed here.

A physical radiation calculation needs more than a vacuum branch. The two harmonic scalar sources in Section 7 violate independent null-space conditions of the Euclidean gravitational Hessian. They rule out the stated linearized edge equations for those fixed sources, including a case that survives removal of the inert diagonal. They do not rule out other discretizations or a fully coupled nonlinear solution. For the axis-time Euclidean branch, conventional ultrarelativistic fermions and the specified minimal coupling give the orientation-independent attenuation bound $a < 1.42 \times 10^{-31}$ m under the conservative energy-fraction and distance inputs. Neither that bound nor the nonbirefringent SME match is transferred to the direct Lorentzian branches.

The next physical connection is consequently specific: construct a matter action and emission vertex consistent with the chosen Lorentzian geometry, then use the polarization-resolved characteristic law over the required directions. The present comparison supplies an exact benchmark for that calculation. Interactions, curved backgrounds and the full quantum integration measure require their own analysis; the free Hessians studied here do not settle those questions.

Author contributions: Conceptualization, J.W.; formal analysis, J.W. and P.B.; writing—original draft preparation, J.W.; writing—review and editing, J.W. and P.B.; visualization, J.W. and P.B.; software, J.W. and P.B.

Acknowledgments: We would like to thank Anil Thapa for reviewing the manuscript and helpful suggestions regarding the scalar model of Section 7.

Funding statement: This research received no external funding.

Conflict of interest statement: The authors declare no conflict of interests.

Data availability statement: No empirical data were analyzed in this study. The numerical programs and their stored outputs form the computational supplement, `https://github.com/jonwashburn/computations/tree/main/papers/2026-10-kuhn-graviton-modes`; the Euclidean programs are also available at https://recognitionphysics.org/qg/lab/#checks as of 2026/11/20.

A The Lorentzian cell and the paired orbit block

This appendix specifies the finite calculation behind Section 6. In a chain simplex use the ordered edge slots $(01, 02, 03, 04, 12, 13, 14, 23, 24, 34)$. For the canonical ordering, $v_i = e_1 + \cdots + e_i$ and the Gram matrix of the four edges from v_0 is $G_{ij} = \min(i, j) - ij$. Each other simplex is its coordinate permutation. Differentiate the positive timelike hinge areas $A_h = \frac{1}{2}\sqrt{-\det G_h}$ and the interior rotation angles of the spacelike normal

planes, on the flat branch described in Section 6. The Schläfli identity removes the area-times-second-angle term from the assembled Hessian. In the squared-edge coordinates of one chain simplex, the space $\mathcal{A}_\sigma$ of Table 2, the cell coefficients are $2\mathsf{Z}/\sqrt{3}$. The matrix Z acts on those ten vertex-pair edges. Here

$$32\mathsf{Z} = \begin{pmatrix} 2 & -2 & 1 & 0 & 0 & 3 & -2 & -6 & 2 & 2 \\ -2 & -4 & 4 & -1 & 6 & -6 & 2 & 3 & -2 & 2 \\ 1 & 4 & 0 & -2 & -6 & 0 & 2 & -3 & 2 & -2 \\ 0 & -1 & -2 & 2 & 2 & 2 & -2 & 2 & -1 & 0 \\ 0 & 6 & -6 & 2 & -6 & 6 & -3 & 0 & 3 & -6 \\ 3 & -6 & 0 & 2 & 6 & 0 & 0 & 6 & -6 & 3 \\ -2 & 2 & 2 & -2 & -3 & 0 & 0 & -6 & 4 & 1 \\ -6 & 3 & -3 & 2 & 0 & 6 & -6 & -6 & 6 & 0 \\ 2 & -2 & 2 & -1 & 3 & -6 & 4 & 6 & -4 & -2 \\ 2 & 2 & -2 & 0 & -6 & 3 & 1 & 0 & -2 & 2 \end{pmatrix}. \tag{123}$$

For edge slot $f = (i, j)$ of simplex π, let $D_{\pi f} = v_j - v_i$ and $m_{\pi f} = (v_i + v_j)/2$. The complete scaled midpoint symbol is

$$(\mathsf{M}_L(q))_{DD'} = \sum_{\substack{\pi \in S_4,\ f, f' \\ D_{\pi f} = D,\ D_{\pi f'} = D'}} 2\mathsf{Z}_{f'f} \cos\bigl(q \cdot (m_{\pi f} - m_{\pi f'})\bigr). \tag{124}$$

Thus the cell table and the 24 coordinate permutations specify every entry of the 15×15 symbol. Pairing opposite midpoint offsets explains the cosine form. In particular, this formula supplies the four coefficients in (81) directly. The momentum covector (x, x, y, y) is unchanged by the swaps $1 \leftrightarrow 2$ and $3 \leftrightarrow 4$. The orbit of an edge is the set of edges reached by those swaps. Edges in one orbit share the counts $(D_1 + D_2, D_3 + D_4)$, and for the non-axis edges each of these count pairs is a single orbit: four edges for $(1, 1)$, two for $(1, 2)$ and for $(2, 1)$, and one each for $(2, 0)$, $(0, 2)$ and $(2, 2)$. A strain invariant under both swaps separately is constant on each orbit. With the axis components set to zero, the six non-axis orbits, in order, are

$$(0, 2),\ (1, 1),\ (1, 2),\ (2, 0),\ (2, 1),\ (2, 2). \tag{125}$$

These strains are the combinations Ωv, where column a of the 15×6 matrix Ω equals 1 on the edges of orbit a and 0 elsewhere.

The matrix $B = \Omega^{\mathsf{T}} \mathsf{M}_L \Omega$ is symmetric and its upper triangle is

$$B = \begin{pmatrix} -2 & -6C_{11} & 2C_{10} & -C_{22} & C_{21} & (1 - C_{20})/2 \\ * & b_{22} & 4C_{01} + 2C_{21} & -6C_{11} & 4C_{10} + 2C_{12} & 2C_{1,-1} - 2C_{11} \\ * & * & C_{20} & C_{12} & 2C_{11} & -3C_{10} \\ * & * & * & -2 & 2C_{01} & (1 - C_{02})/2 \\ * & * & * & * & C_{02} & -3C_{01} \\ * & * & * & * & * & 3 \end{pmatrix}, \tag{126}$$

where $C_{pq} = \cos((px+qy)/2)$ and $b_{22} = -8 - 6C_{02} - 6C_{20} - 4C_{22}$. Substituting $x = z + t$, $y = z - t$ and expanding its determinant gives

$$\det B(z+t, z-t) = -36 \sin^2 \frac{z+t}{2} \sin^2 \frac{z-t}{2} P(\cos z, \cos t), \tag{127}$$

with

$$\begin{aligned} \Pi(r,s) = {} & 16r^6 - 8sr^5 - 8s^2r^4 - 42r^4 + 2s^3r^3 + 39sr^3 \\ & + 3s^2r^2 + 25r^2 - s^3r - 35sr + 7s^2 + 2. \end{aligned} \tag{128}$$

The identity $P(1-2V, 1-2U) = G_+(U,V)$ yields (85). It can be checked as an ordinary polynomial identity after replacing the cosines in (126) by half-angle exponentials. The sine prefactors are nonzero near $z = \sqrt{3}t$ for small positive t.

To see why a block zero mode is a full zero mode, note first that swap invariance makes all residual entries within each orbit equal. A zero orbit sum therefore kills each non-axis residual. The Bianchi identity contracts the remaining residual with every vertex displacement; its coefficients on the axis edges are the diagonal factors $4\mathrm{i}\sin(q_\mu/2)\xi_\mu$. Where these factors are nonzero, every remaining residual vanishes. The same diagonal factors fix the gauge uniquely on the axis edges. A nonzero block zero mode is consequently nongauge. This supplies the reconstruction used in the main text, without treating a gauge-fixed determinant root alone as a propagating mode.

B The computation

The numerical and symbolic computations in this paper are reproducible with the Python programs of its computational supplement, `https://github.com/jonwashburn/computations/tree/main/papers/2026-10-kuhn-graviton-modes`, which also stores the output of each program. The Euclidean programs are available for download at `https://recognitionphysics.org/qg/lab/#checks` as of 2026/11/20. In this appendix we give additional details about these calculations.

Exact gradients.

Squared edge lengths are the coordinates. For each of the 50 hinge classes at the origin the area gradient $\partial A_h/\partial a_e$ is read from Heron's formula and the deficit gradient $\partial\delta_h/\partial a_e$ from the interior dihedral angles of the simplices containing the hinge. If G is the 4×4 Gram matrix of edges from one simplex vertex, then $G_{ij} = (a_{0i} + a_{0j} - a_{ij})/2$ and, for opposite faces indexed by $i, j > 0$,

$$\cos\theta_{ij} = -\frac{(G^{-1})_{ij}}{\sqrt{(G^{-1})_{ii}(G^{-1})_{jj}}}. \tag{129}$$

The minus sign chooses the interior angle. Relabeling vertices covers the remaining faces. Equivalently, squared simplex volumes come from the Cayley–Menger determinant, $V_d^2 = (-1)^{d+1} \det \mathrm{CM}/[2^d (d!)^2]$; its cofactors determine the same dihedral cosines.

Differentiating these formulas and the area formula gives the Hessian weights. Both are evaluated symbolically at the flat configuration, where they are algebraic numbers, and then to sixty digits. Assembling (4) with the translation phases of (8) gives 302 nonzero couplings (D, D', v), v the midpoint separation; every coupling weight is a rational number (the square roots in the individual gradients cancel in the products $\partial A\,\partial\delta$ summed over hinges), taking only the values $-\frac{3}{2}$ (4), -1 (6), $-\frac{1}{2}$ (4), $\frac{1}{2}$ (48), $\frac{1}{4}$ (96) and $-\frac{1}{4}$ (144); the census by squared lengths $(|D|^2, |D'|^2)$ is $(1,1)$:52, $(1,2)$:96, $(1,3)$:48, $(2,2)$:54, $(2,3)$:48, $(3,3)$:4, and none touch the hypercube diagonal. The reflection asymmetry $\max|w(D,D',v) - w(D,D',-v)|$ is exactly 0, which is Lemma 2.2(i) at the level of the table. The deficit gradient $\partial\delta_h/\partial a_{1111}$ has 54 nonzero entries and the area gradient $\partial A_h/\partial a_{1111}$ none, which is Theorem 3.1 at the level of the table.

Finite-difference check.

Independently of the gradient formulas, the full nonlinear Regge action was evaluated in double precision on a 4^4 periodic Kuhn lattice with $15 \cdot 4^4$ edges, perturbed by a plane-wave strain of amplitude ϵ in six commensurate modes, and its Richardson-extrapolated second difference in ϵ ($\epsilon = 3 \times 10^{-3}$ and 1.5×10^{-3}) compared with $\frac{1}{2}c^{\mathsf{T}}\mathsf{M}(k)c$. The relative differences are 3×10^{-11} to 1.6×10^{-8}, the size of double-precision roundoff in the 12,800 deficit angles divided by ϵ^2.

Exact certificates.

All 302 coupling weights are rational numbers. A separate program works in exact rational arithmetic from the coupling table: the characteristic polynomial of $\mathsf{M}(0)$ is $\lambda^{11}(\lambda+2)^3(\lambda+8)$ (Proposition 3.2); the hypotenuse row of M_0 and of $\mathsf{M}_2(u)$ is zero (Theorem 3.1); $P^{\mathsf{T}}\mathsf{M}_0' = 0$; and $P^{\mathsf{T}}\mathsf{M}_2'(u)P + \frac{1}{4}G(u)$, expanded symbolically in $u_1, \dots, u_4$ in the unnormalized coordinates $h_{\mu\nu}$, is the zero 10×10 matrix (Theorem 3.4). As a numerical cross-check, $\mathsf{E}_2(u)$ from the forty-digit Schur-complement series was formed at twelve $u \in \mathbb{C}^4$ with real and imaginary parts uniform in $[-1.5, 1.5]$ and compared entrywise with $-\frac{1}{4}G(u)$ in Frobenius coordinates; the largest entry of the difference is 4.9×10^{-41}, and the 12×10 matrix of monomials $u_\alpha u_\beta$ at those points has smallest singular value 0.549.

Reduction and expansion.

The Schur complement (14) is formed exactly as a trigonometric matrix for the root searches, and as a Taylor series in u to order six for the expansions, by series inversion of $D_Q(u) = Q^{\mathsf{T}}\mathsf{M}'(u)Q$. Metric coordinates are Frobenius orthonormal ($x_{\mu\mu} = h_{\mu\mu}$, $x_{\mu\nu} = \sqrt{2}h_{\mu\nu}$ for $\mu < \nu$). In a frame $(T, \hat{n})$ with $u = \mathrm{i}T + \hat{n}$ the two TT polarizations are $(aa - bb)/\sqrt{2}$ and $(ab + ba)/\sqrt{2}$ for a, b an orthonormal basis of the plane orthogonal to T and $\hat{n}$; the four leading gauge vectors are $u \otimes e_\mu + e_\mu \otimes u$. The on-shell operator Λ of Corollary 5.3 is the quartic coefficient of the 2×2 Schur complement of the Taylor-expanded $\mathsf{E}(u)$ onto the polarizations, which requires E_2 to annihilate the leading gauge vectors exactly ($|\mathsf{E}_2 g_0| < 4 \times 10^{-41}$) and $\mathsf{E}_4 g_0$ to be orthogonal to the polarizations ($|\tau_{+,\times}^{\mathsf{T}}\mathsf{E}_4 g_0| < 4 \times 10^{-41}$); both hold.

Root search.

Let U be the 10×2 matrix of Corollary 5.3, whose columns are the Frobenius coordinates of τ_+ and $\tau_\times$. For a frame $(T,\hat n)$, form the four gauge vectors $g_\mu = u\otimes e_\mu + e_\mu\otimes u$ at $u = \mathrm{i}T+\hat n$. Orthonormalize the standard basis of $\mathbb{C}^{10}$ against the two columns of U. Keep a vector from that list whenever those two columns, the four gauge vectors and the vectors already kept have smallest singular value above 10^{-12}, and stop at four vectors. Let W be the 10×6 matrix with the columns of U first and these four vectors after them. The four are orthonormal and orthogonal to τ_+ and $\tau_\times$, and linearly independent from the gauge vectors. W is fixed for the frame. Partition the Gram matrix of $\mathsf{E}(u)$ on these columns as

$$F(u) = W^{\mathsf{T}}\mathsf{E}(u)W = \begin{pmatrix} F_{11}(u) & F_{12}(u) \\ F_{21}(u) & F_{22}(u) \end{pmatrix}, \tag{130}$$

with F_{11} the 2×2 block on the columns of U, F_{22} the 4×4 block on the four kept columns, and F_{12}, F_{21} the off-diagonal blocks. Eliminating the four columns gives

$$D_{\mathrm{TT}}(u) = F_{11}(u) - F_{12}(u)\,F_{22}(u)^{-1}F_{21}(u), \tag{131}$$

and $\lambda_{\min}(u)$ is the eigenvalue of $D_{\mathrm{TT}}(u)$ of smallest modulus. For Table 4, ω is the root of $\lambda_{\min}(\mathrm{i}\omega T+\mathrm{k}\hat n)=0$ returned by `mpmath.findroot`, started at the root of $\mathcal{L}(u)=0$, with tolerance 10^{-30}. The singular values of the 10×10 matrix E at that root are an independent check. A separate secant iteration on $\lambda_{\min}$, started from the quartic prediction and stopped below residual 10^{-32}, produces $\kappa = (1-\omega/\mathrm{k})/\mathrm{k}^2$ at $\mathrm{k}=0.1$ and $\mathrm{k}=0.05$. Its Richardson extrapolation reproduces $(1+A)/24$ to 5×10^{-8} in four directions; the residual is the $O(\mathrm{k}^6)$ term of (47).

Random complex u.

Eight $u\in\mathbb{C}^4$ with real parts in $[-2.5,2.5]$ and imaginary parts in $[-1.5,1.5]$; for four of them u_4 was replaced by $2\arcsin(\mathrm{i}\sqrt{\sum_{\mu\le3}\sin^2(u_\mu/2)})$, which puts u on $\mathcal{L}=0$. The nullity of the 15×15 symbol (singular values below 10^{-30}) was 5 in the first four cases and 7 in the last four, and the body-diagonal block of the symbol was $-\frac12 I_4$ in every trial, as it is at every k.

Direction scan.

For Theorem 5.4, κ was evaluated from (68) at 2000 uniformly random unit $\hat n\perp T$ for each of the four time directions. Observed ranges of 24κ: axis $[1.335,1.998]$ (proved $[4/3,2]$); face $[-1.995,1.489]$ (proved $[-2,3/2]$); body $\mathrm{Re}\in[-1.167,1.330]$ (proved $[-7/6,4/3]$), $|\mathrm{Im}|\le0.935$ (proved $\le2\sqrt2/3=0.943$); hypercube $\mathrm{Re}\in[-0.992,-0.669]$ (proved $[-1,-2/3]$), $|\mathrm{Im}|\le1.142$ (proved $\le2/\sqrt3=1.155$). Every sample lies inside its proved range and the samples approach the endpoints.

Spherical components.

With $A(\hat n)=\sum_j n_j^4$, the projections onto the standard spherical harmonics (unit normalized on the sphere; A is real and even in the azimuth, so $\langle A,Y_{44}\rangle=\langle A,\mathrm{Re}\,Y_{44}\rangle$)

give

$$A(\hat{n}) = \frac{3}{5} + \frac{4\sqrt{\pi}}{15}\Big[Y_{40}(\hat{n}) + \sqrt{\tfrac{5}{14}}\big(Y_{44}(\hat{n}) + Y_{4,-4}(\hat{n})\big)\Big], \tag{132}$$

which at $\hat{n}$ along an axis gives $\frac{3}{5} + \frac{4\sqrt{\pi}}{15} \cdot \frac{3}{2\sqrt{\pi}} = 1$ as it must. Equation (112) follows by substituting this into (109) and (110), using the substitution $Y_{00} = \frac{1}{2\sqrt{\pi}}$ to put the constants in terms of Y_{00}. The ratio $s_{44}/s_{40} = \sqrt{5/14} = 0.5976$ is fixed by cubic symmetry and is the same for any cubic lattice theory whose anisotropy is carried by a single $j = 4$ invariant.

Constants.

$E_{\mathrm{P}} = 1.220890 \times 10^{19}$ GeV, $\ell_{\mathrm{P}} = 1/E_{\mathrm{P}} = 1.616 \times 10^{-35}$ m, 1 m $= 5.0677 \times 10^{15}\,\mathrm{GeV}^{-1}$, 1 Mpc $= 3.0857 \times 10^{22}$ m.

The original numerical run uses 40 decimal digits and gradients at 60. The supplied checks have separate roles:

- `regge_4d_quartic_tt_dispersion_20260903.py` builds the geometric Hessian and performs the numerical checks, using the three geometry modules supplied beside it.
- `regge_4d_exact_quadratic_identity_20260904.py` verifies the zero-momentum and quadratic identities in rational arithmetic.
- `VerifyCurrentDraft.py` verifies all 100 entries of $W^\sharp R W + \frac{1}{2}(\mathcal{L}V - C^\sharp C) = 0$ in the squared-edge coordinates used here, as well as the gauge map and $CV^{-1}C^\sharp = \mathcal{L}I_4$ as rational-function identities.
- `VerifyScalarCoupling.py` checks the simplex scalar reduction, metric derivatives and assembled vertex variation in Section 7.
- `VerifyQuartic.py` forms the full five-dimensional off-shell TT restriction and diagonalizes it exactly, including off-diagonal entries.

The direct Lorentzian comparison of Section 6 has its own programs. They start from the vertex coordinates of the Kuhn simplices on $g_L = I_4 - J_4$ and read no stored table.

- `appendixA_cell.py` computes the squared intervals, the timelike hinge areas, the interior angles and their first derivatives in exact arithmetic, and from them the Hessian cell. It checks the cell against (123) entry by entry, the assembly rule (124), the angle sum 2π around each of the 50 hinge classes and the gauge identity $\mathsf{M}_L(q)g_\xi(q) = 0$. Run on the Euclidean background, the same code reproduces the 302-coupling table described above.
- `section6_paired_direction.py` assembles M_L from that cell and checks (78)–(86), the block (126) and the determinant (127) in exact arithmetic. At $K = 0.1$ it reconstructs the cross and plus zero modes of the full 15×15 symbol to fifty digits and confirms that neither is a gauge vector.
- `section7_source_constraints.py` computes both contractions of Section 7, $-\kappa_m\lambda^2/12$ and $g^{\mathsf{T}}J = -18\kappa_m\lambda^2$, the second both from (98) and by displacing the vertex directly.

- `sections8_9_bound_numbers.py` recomputes the numbers of Sections 8 and 9 from the constants above.

Each of these programs stores its complete output, and a run record lists the SHA-256 hash of every program and output file.

The supplementary instructions name the dependencies, commands and stored output files. The stored output of `VerifyCurrentDraft.py` records the manuscript and input-table hashes; it checks the listed identities, not every sentence of the paper. The raw, unsymmetrized geometric assembly also agrees with the supplied table and satisfies reciprocity before any averaging. This independently checks the Hessian symmetry described in Section 2.

References

[1] Regge, T.: General relativity without coordinates. Il Nuovo Cimento **19**(3), 558–571 (1961) https://doi.org/10.1007/BF02733251

[2] Gentle, A.P.: Regge calculus: A Unique tool for numerical relativity. Gen. Rel. Grav. **34**, 1701–1718 (2002) https://doi.org/10.1023/A:1020128425143 arXiv:gr-qc/0408006

[3] Loll, R.: Quantum gravity from causal dynamical triangulations: A review. Classical and Quantum Gravity **37**, 013002 (2020) https://doi.org/10.1088/1361-6382/ab57c7 arXiv:1905.08669

[4] Perez, A.: The spin foam approach to quantum gravity. Living Reviews in Relativity **16**, 3 (2013) https://doi.org/10.12942/lrr-2013-3 arXiv:1205.2019

[5] Feinberg, G., Friedberg, R., Lee, T.D., Ren, H.C.: Lattice gravity near the continuum limit. Nuclear Physics B **245**, 343–368 (1984) https://doi.org/10.1016/0550-3213(84)90436-X

[6] Beane, S.R., Davoudi, Z., Savage, M.J.: Constraints on the Universe as a Numerical Simulation. Eur. Phys. J. A **50**(9), 148 (2014) https://doi.org/10.1140/epja/i2014-14148-0 arXiv:1210.1847 [hep-ph]

[7] Freudenthal, H.: Simplizialzerlegungen von beschränkter flachheit. Annals of Mathematics **43**(3), 580–582 (1942) https://doi.org/10.2307/1968813

[8] Kuhn, H.W.: Some combinatorial lemmas in topology. IBM Journal of Research and Development **4**(5), 518–524 (1960) https://doi.org/10.1147/rd.45.0518

[9] Roček, M., Williams, R.M.: Quantum Regge calculus. Physics Letters B **104**(1), 31–37 (1981) https://doi.org/10.1016/0370-2693(81)90848-0

[10] Roček, M., Williams, R.M.: The quantization of Regge calculus. Zeitschrift für Physik C: Particles and Fields **21**(4), 371–381 (1984) https://doi.org/10.1007/

BF01581603

[11] Williams, R.M.: Quantum Regge calculus in the Lorentzian domain and its Hamiltonian formulation. Classical and Quantum Gravity **3**(5), 853–869 (1986) https://doi.org/10.1088/0264-9381/3/5/015

[12] Williams, R.M., Tuckey, P.A.: Regge calculus: a brief review and bibliography. Classical and Quantum Gravity **9**(5), 1409–1422 (1992) https://doi.org/10.1088/0264-9381/9/5/021

[13] Loll, R.: Discrete approaches to quantum gravity in four dimensions. Living Reviews in Relativity **1**, 13 (1998) https://doi.org/10.12942/lrr-1998-13 arXiv:gr-qc/9805049

[14] Hamber, H.W.: Quantum gravity on the lattice. General Relativity and Gravitation **41**, 817–876 (2009) https://doi.org/10.1007/s10714-009-0769-y arXiv:0901.0964 [gr-qc]

[15] Kostelecký, V.A., Tasson, J.D.: Constraints on Lorentz violation from gravitational čerenkov radiation. Physics Letters B **749**, 551–559 (2015) https://doi.org/10.1016/j.physletb.2015.08.060 arXiv:1508.07007 [gr-qc]

[16] Bahr, B., Dittrich, B.: (Broken) Gauge Symmetries and Constraints in Regge Calculus. Class. Quant. Grav. **26**, 225011 (2009) https://doi.org/10.1088/0264-9381/26/22/225011 arXiv:0905.1670 [gr-qc]

[17] Wald, R.M.: General Relativity. University of Chicago Press, ??? (1984)

[18] Carroll, S.M.: Spacetime and Geometry: An Introduction to General Relativity. Cambridge University Press, Cambridge, UK (2019). https://doi.org/10.1017/9781108770385

[19] Montvay, I., Munster, G.: Quantum Fields on a Lattice. Cambridge University Press, Cambridge (1997). https://doi.org/10.1017/CBO9780511470783 . Cambridge Monographs on Mathematical Physics

[20] Borissova, J.N., Dittrich, B.: Lorentzian quantum gravity via Pachner moves: one-loop evaluation. JHEP **09**, 069 (2023) https://doi.org/10.1007/JHEP09(2023)069 arXiv:2303.07367 [hep-th]

[21] Kostelecký, V.A., Mewes, M.: Testing local Lorentz invariance with gravitational waves. Physics Letters B **757**, 510–514 (2016) https://doi.org/10.1016/j.physletb.2016.04.040 arXiv:1602.04782 [gr-qc]

[22] Moore, G.D., Nelson, A.E.: Lower bound on the propagation speed of gravity from gravitational Cherenkov radiation. Journal of High Energy Physics **2001**(09), 023 (2001) https://doi.org/10.1088/1126-6708/2001/09/023 arXiv:hep-ph/0106220

[23] Tiesinga, E., Mohr, P.J., Newell, D.B., Taylor, B.N.: CODATA recommended values of the fundamental physical constants: 2018. Reviews of Modern Physics **93**(2), 025010 (2021) https://doi.org/10.1103/RevModPhys.93.025010

[24] Bird, D.J., *et al.*: Detection of a cosmic ray with measured energy well beyond the expected spectral cutoff due to cosmic microwave radiation. The Astrophysical Journal **441**, 144–150 (1995) https://doi.org/10.1086/175344 arXiv:astro-ph/9410067

[25] Aab, A., *et al.*: Depth of maximum of air-shower profiles at the Pierre Auger Observatory. II. composition implications. Physical Review D **90**(12), 122006 (2014) https://doi.org/10.1103/PhysRevD.90.122006 arXiv:1409.5083 [astro-ph.HE]

[26] Bekenstein, J.D.: Black holes and entropy. Phys. Rev. D **7**, 2333–2346 (1973) https://doi.org/10.1103/PhysRevD.7.2333

[27] Hawking, S.W.: Black hole explosions. Nature **248**, 30–31 (1974) https://doi.org/10.1038/248030a0

[28] Washburn, J.: Gravity in Recognition Science: Results, Consistency Tests, and Open Problems — September 2026. (2026). https://doi.org/10.5281/zenodo.22850335 . https://doi.org/10.5281/zenodo.22850335

[29] Mukhanov, V.F.: Are black holes quantized? Soviet Journal of Experimental and Theoretical Physics Letters **44**, 63–66 (1986)

[30] Hooft, G.: Dimensional reduction in quantum gravity. Conf. Proc. C **930308**, 284–296 (1993) arXiv:gr-qc/9310026

[31] Bekenstein, J.D., Mukhanov, V.F.: Spectroscopy of the quantum black hole. Phys. Lett. B **360**, 7–12 (1995) https://doi.org/10.1016/0370-2693(95)01148-J arXiv:gr-qc/9505012

[32] Washburn, J.: Gravity and Light on One Lattice: The gravitational-wave sector of Recognition Science: one speed shared with light and tested by GW170817, zero graviton mass, two polarizations, and a cosmic-ray window on the lattice scale. Zenodo (2026). https://doi.org/10.5281/zenodo.22680040 . https://doi.org/10.5281/zenodo.22680040

[33] Washburn, J.: Native Photon Propagation and Its Lorentz Limit. (2026). https://doi.org/10.5281/zenodo.22850196 . https://doi.org/10.5281/zenodo.22850196